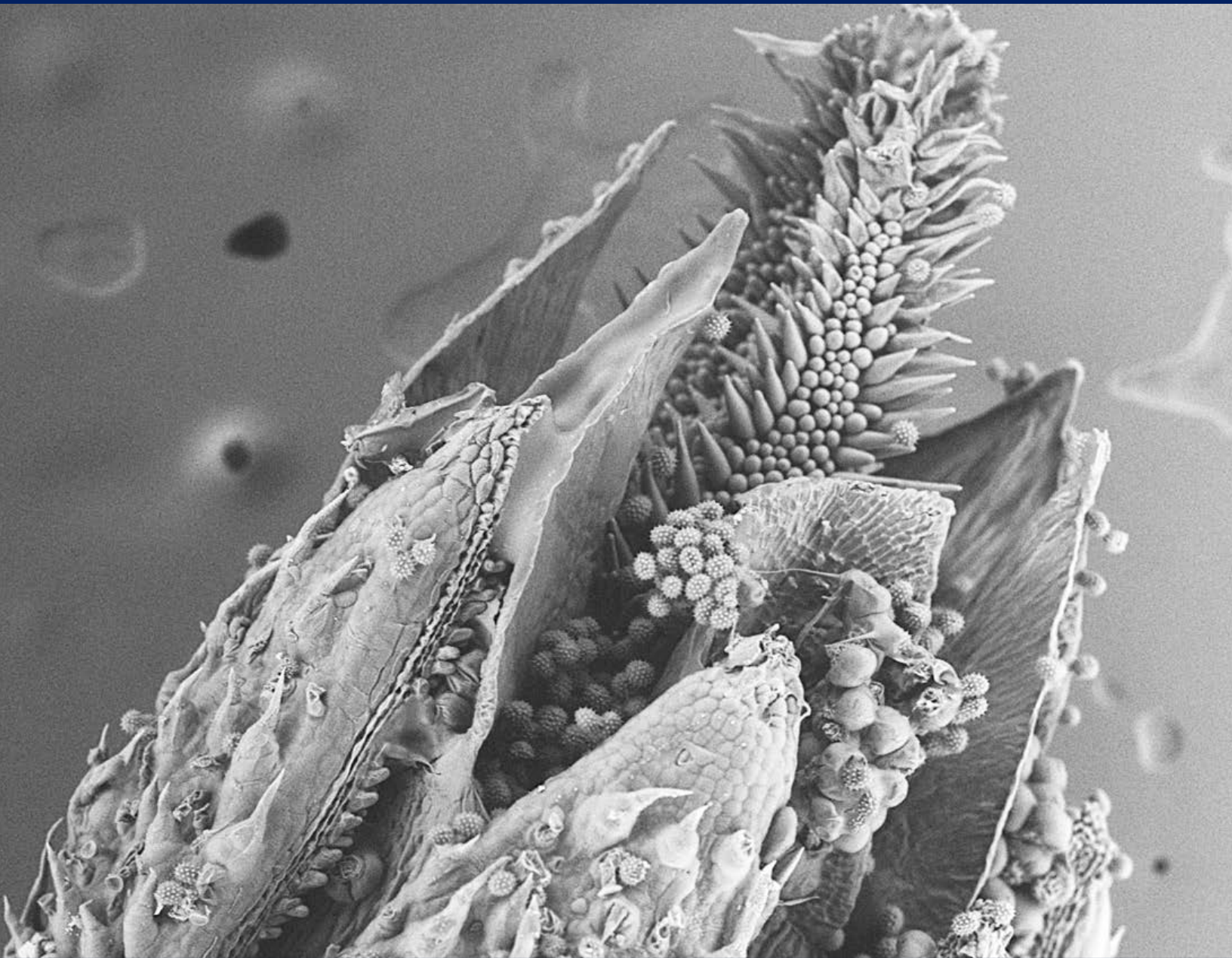
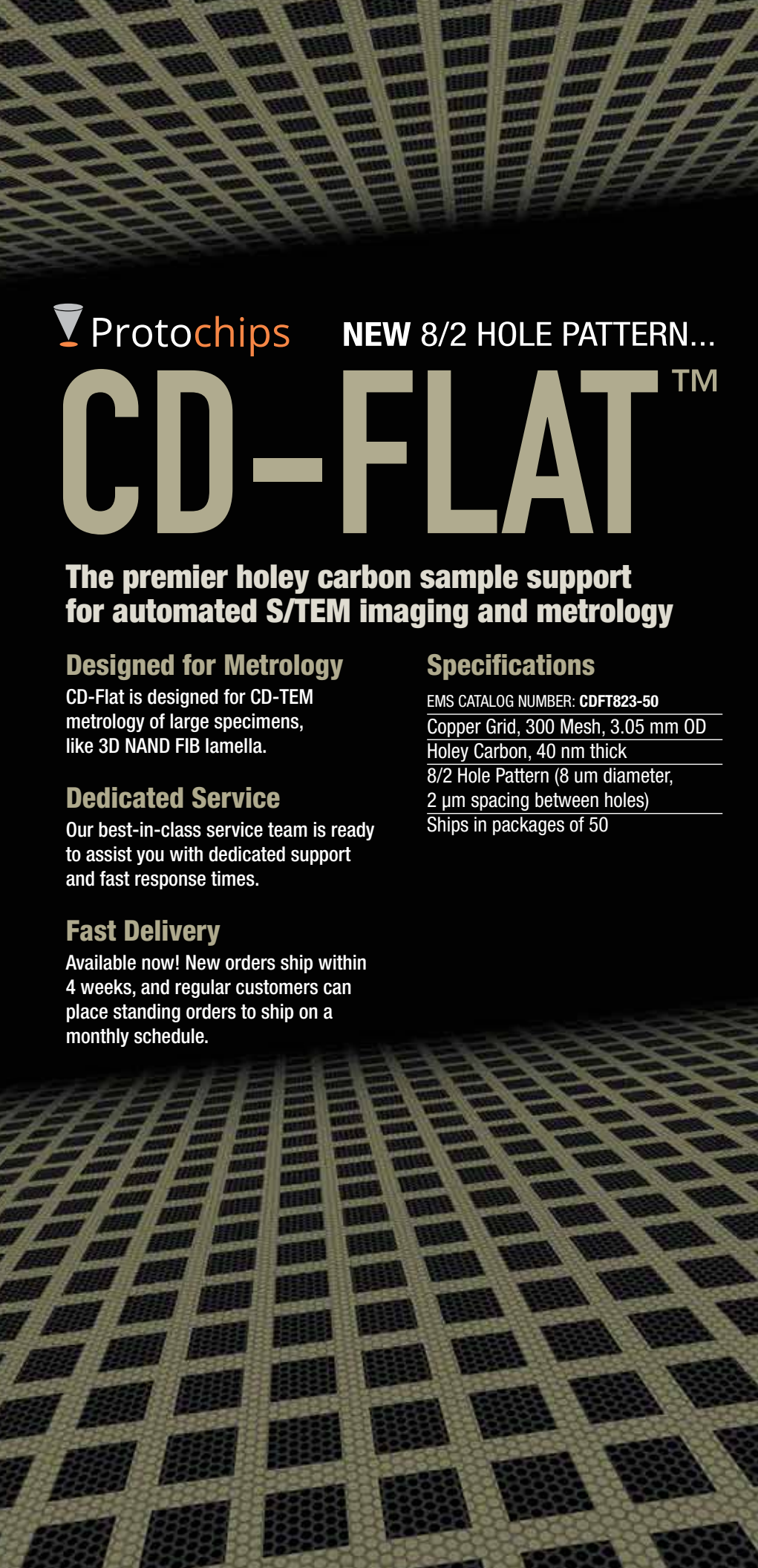


# *Texas Journal of Microscopy*



Volume 51  
Number 1, 2020  
ISSN 1554-0820

Visit our website at [www.texasmicroscopy.org](http://www.texasmicroscopy.org)



Protochips **NEW 8/2 HOLE PATTERN...**

# CD-FLAT™

**The premier holey carbon sample support for automated S/TEM imaging and metrology**

## Designed for Metrology

CD-Flat is designed for CD-TEM metrology of large specimens, like 3D NAND FIB lamella.

## Dedicated Service

Our best-in-class service team is ready to assist you with dedicated support and fast response times.

## Fast Delivery

Available now! New orders ship within 4 weeks, and regular customers can place standing orders to ship on a monthly schedule.

## Specifications

EMS CATALOG NUMBER: **CDFT823-50**

Copper Grid, 300 Mesh, 3.05 mm OD

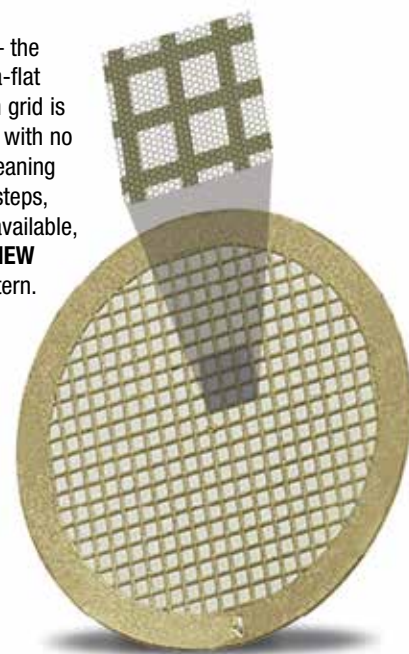
Holey Carbon, 40 nm thick

8/2 Hole Pattern (8  $\mu$ m diameter, 2  $\mu$ m spacing between holes)

Ships in packages of 50

**The C-flat™ advantage in a new pattern**

CD-flat™ — the premier ultra-flat holey carbon grid is ready to use with no additional cleaning or handling steps, and is now available, featuring a **NEW** 8/2 hole pattern.



**PLEASE CONTACT US FOR MORE INFORMATION...**

# EMS has it!

## Electron Microscopy Sciences

P.O. Box 550 • 1560 Industry Rd.  
Hatfield, Pa 19440  
Tel: (215) 412-8400 • Fax: (215) 412-8450  
email: [info@emsdiasum.com](mailto:info@emsdiasum.com)  
*or* [stacie@ems-secure.com](mailto:stacie@ems-secure.com)

OUR MAIN INTERACTIVE WEBSITE:  
**[www.emsdiasum.com](http://www.emsdiasum.com)**

Follow us on...



## TSM OFFICERS 2019-2020

**President:**

BERND ZECHMANN  
Center for Microscopy and Imaging  
Baylor University • Waco, TX 76798-7046  
(254) 710-2322 • Bernd\_Zechmann@baylor.edu

**President-elect:**

VACANT

**Past President:**

LAURA HANSON  
Department of Biology  
Texas Woman's University • Denton, TX 76204-5799  
(940) 898-2472 • LHanson@twu.edu

**Secretary:**

Shazia Ahmed  
Department of Biology  
Texas Woman's University • Denton, TX 76204-5799  
(940) 898-2390 • SAhmed@twu.edu

**Secretary-elect:**

VACANT

**Treasurer:**

DAVID GARRETT  
Dept. of Materials Science and Engineering  
University of North Texas • Denton, Texas 76203-5017  
(940) 369-8836 • dgarrett@unt.edu

**Treasurer-elect:**

VACANT

**Program Chairwoman:**

JOSEFINA ARELLANO-JIMENEZ  
The University of Texas at Dallas • Dallas, TX 75080  
(210) 458-8735 • josefina.arellano@utdallas.edu

**Program Chairwoman-elect:**

VACANT

## APPOINTED OFFICERS

**Corporate Member Representative:**

JAMES LONG  
Ted Pella, Inc.  
P.O. Box 492477 • Redding, CA 96049  
(530) 227-8329 • james\_long@tedpella.com

**Facebook Master:**

NABARUN GHOSH  
Dept. of Life, Earth, and Environmental Sciences  
West Texas A&M University  
Canyon, Texas 79015  
(806) 651-2571 • fax (806) 651-2928  
nghosh@wtamu.edu

**Student Representative:**

AUBREY HOWARD  
West Texas A&M University • Canyon, Texas 79015  
(806) 632-9759 • adhoward3@buffs.wtamu.edu

**Journal Editors:**

CATALINA PISLARIU  
Department of Biology  
Texas Woman's University • Denton, TX 76204-5799  
(940) 898-4611 • cpislariu@twu.edu

**Webmaster:**

BERND ZECHMANN  
Center for Microscopy and Imaging  
Baylor University • Waco, TX 76798-7046  
(254) 710-2322 • Bernd\_Zechmann@baylor.edu

# Contents



TEXAS JOURNAL OF MICROSCOPY  
VOLUME 51, NUMBER 1, 2020  
ISSN 1554-0820

*Editor*

Catalina Pislariu, PhD  
Department of Biology, Texas Woman's University, Denton, TX 76204

**Official Journal of the Texas Society for Microscopy**

*"TSM - Embracing all forms of Microscopy"*

[www.texasmicroscopy.org](http://www.texasmicroscopy.org)

President's Message .....	5
Keynote Speakers for the 55th TSM Meeting .....	6
Spring 2020 Life Sciences Abstracts.....	8
Spring 2020 Material Sciences Abstracts.....	17
Spring 2020 Education/Life Sciences Abstracts .....	19
Spring 2020 Technical Abstracts .....	21
Spring 2020 Short Communications .....	24
Spring 2020 Full Articles .....	26
Corporate Members .....	32

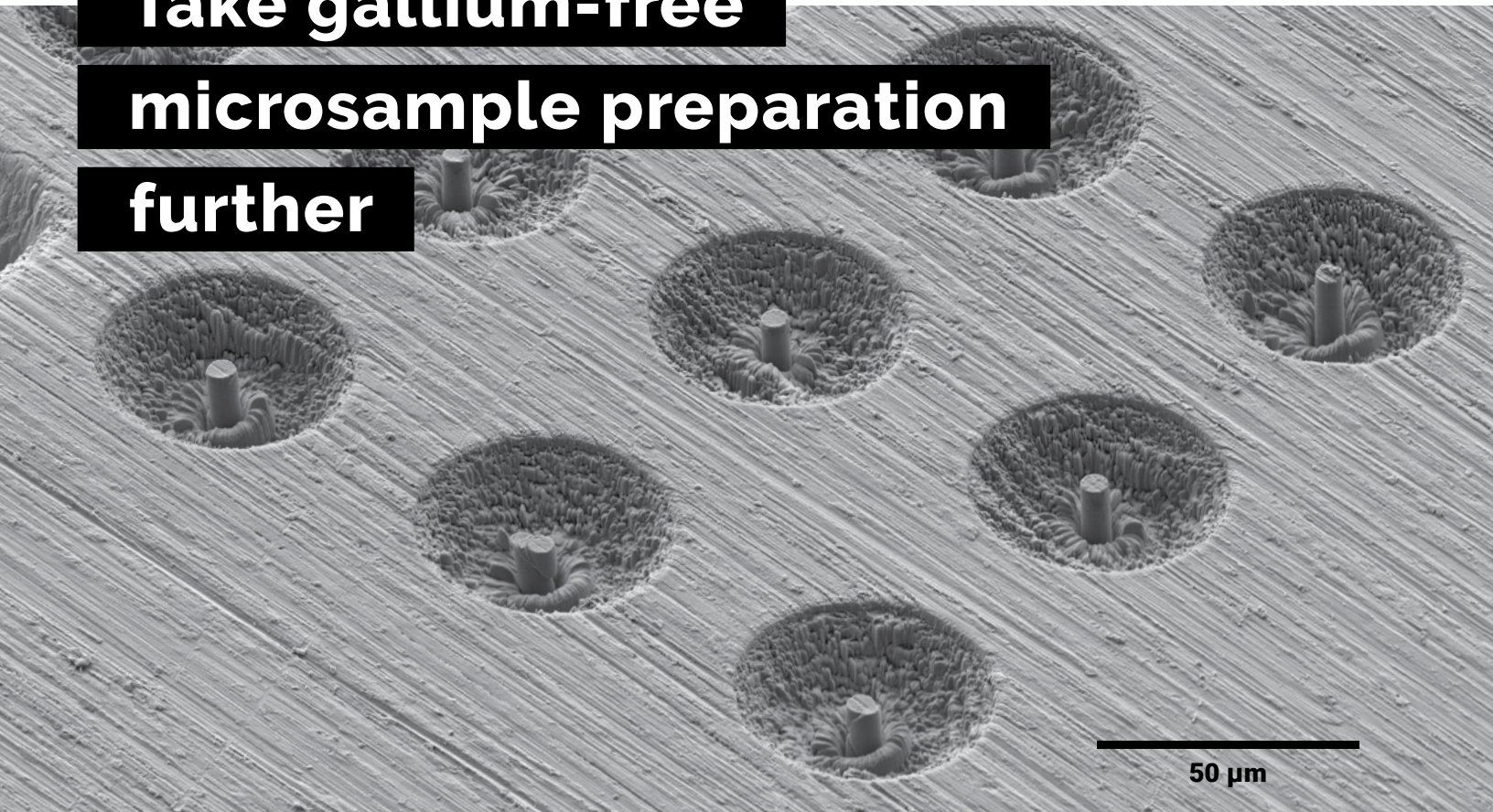
Advertiser's Index:

Electron Microscopy Sciences/ProtocChips.....	2
Tescan.....	4
Electron Microscopy Sciences .....	34
Diatome .....	36

## ON THE COVER

The morpho-anatomy of sunflower (*Helianthus annuus*, Asteraceae) disk floret visualized with a Hitachi TM-1000 SEM. The pistillate disk floret shows the cylindrical corolla with trichomes, anther tips inside the corolla, stigma in the center and pollen on all organs. Micrograph taken by Jennie Wojtaszek, former graduate student in Camelia Maier's lab in the Department of Biology at Texas Woman's University and past TSM Student Representative and Secretary.

# Take gallium-free microsample preparation further



Array of micro-compression test pillars in UFG aluminium alloy

## TESCAN AMBER X

- ✓ High throughput, large area FIB milling up to 1 mm
- ✓ Ga-free microsample preparation
- ✓ Ultra-high resolution, field-free FE-SEM imaging and analysis
- ✓ In-column SE and BSE detection
- ✓ Spot optimization for high-throughput, multi-modal FIB-SEM tomography
- ✓ Superior field of view for easy navigation
- ✓ Essence™ easy-to-use, modular graphical user interface



For more information visit

[www.tescan.com](http://www.tescan.com)

---

---

# President's Message

---

**T**he Executive Council of the Texas Society for Microscopy (TSM) can look back on a very successful year. In August, Josefina Arellano Jimenez and I represented our society at the M & M meeting in Portland. In October, the Microanalysis Society (MAS) accepted our application to become a local affiliated society (LAS). As an affiliated society, we can apply for a renowned tour speaker free of charge for our annual meeting. In order to keep our status of LAS, 10% of our members need to be members of the MAS, and I encourage all of our members to renew or apply for new MAS-membership for 2020.

In addition, the TSM is a local affiliated society of the Microscopy Society of America (MSA), which also has many advantages. For example, in October we decided to join the LAS website project. Through a strategic initiative grant sponsored by the MSA, our website will get a new look. The new webpage ([www.texas.microscopy.org](http://www.texas.microscopy.org)) will go online in March 2020, be fully encrypted and compatible with mobile devices, and future maintenance will be free of charge.

Being part of the MAS and MSA saved us quite a lot of money in 2019 which we were able to turn around and spend on our student members. In 2019, we were able to provide sixteen student members with travel support to attend the meeting in San Antonio. We were also able to support the research of Luis Grado, undergraduate student at Sam Houston State University, and Sukbir Kaur, a graduate student at Texas Woman's University, with our Small Grant Program. As the TSM is in good financial health, the executive council has decided to increase travel support for students who are giving a presentation at the annual meeting from \$100 to \$200.

The 55th annual meeting in College Station is on track to being a magnificent meeting with fabulous workshops. Josefina Arellano Jimenez has done an excellent job of organizing the meeting together with Stan Vitha, our local organizer at Texas A & M University. I want to thank them both for their hard work. I also want to thank Electron

Microscopy Sciences, Leica Microsystems and Tescan for sponsoring these workshops, and for showing our members the latest advances in sample preparation and analysis. I also want to express my thanks to our editor, Catalina Pislariu, for preparing, designing and publishing the 51st issue of the Texas Journal of Microscopy.

I am very grateful for the support of all the officers on the executive board who have spent countless hours to keep the TSM going. I want to thank Shazia Ahmed who does an amazing job in her role as secretary of the TSM. I also want to express my thanks to David Garrett for keeping up with our finances throughout the year. Further, I want to thank James Long who does a great job representing our corporate members, and Aubrey Howard who does an amazing job getting students involved in the TSM. I want to thank Nabarun Ghosh who has done a wonderful job increasing the visibility of the TSM on our social networks and for organizing the 56th TSM meeting at West Texas A&M University in Canyon in 2021.

Finally, I want to thank all corporate, honorary, regular, and student members for supporting the TSM with their membership and for participating at our annual meetings. It has been a great honor and pleasure to serve you in the capacity of the TSM President, and I am excited to continue to share my enthusiasm for microscopy with our members.

Bernd Zechmann  
TSM President 2019-2020



# TEXAS SOCIETY FOR MICROSCOPY'S 55TH ANNUAL MEETING

## KEYNOTE SPEAKER PRESENTATIONS

### 3-D, IN-SITU, AND ULTRAFAST ELECTRON MICROSCOPY

**ILKE ARSLAN**

**Interim Division Director, Nanoscience and Technology  
Center for Nanoscale Materials, Argonne National Laboratory**



With recent advances in *in-situ* microscopy, a new era in microscopy has arrived that allows for the dynamic imaging of materials under reaction conditions in the (scanning) transmission electron microscope. It is no longer sufficient to image materials under vacuum conditions, but to get closer to the conditions in which the material will be used, such as high/low temperature, liquid environments, gas environments, or a combination thereof. Within these environments, moving beyond “real time” imaging to ultrafast imaging can provide yet another level of fundamental understanding of nanomaterials. Further, combining an *in-situ* or *ex-situ* experiment with electron tomography is a very powerful method for materials characterization as this provides the 3-D morphology/chemistry of the materials in more relevant environments. This talk will focus on newer developments such as *in-situ* heating in liquid, reconstruction algorithms for electron tomography with significantly fewer images, and the future of ultrafast transmission electron microscopy at the Center for Nanoscale Materials.



# TEXAS SOCIETY FOR MICROSCOPY'S 55TH ANNUAL MEETING

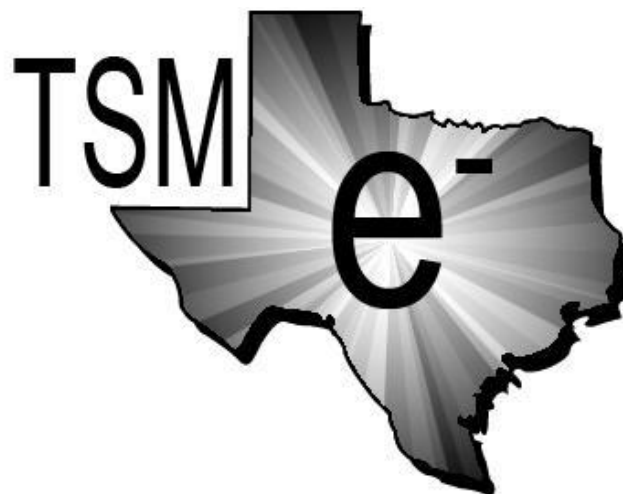
## KEYNOTE SPEAKER PRESENTATIONS

### IMAGING SUBCELLULAR DYNAMICS IN THREE DIMENSIONS

**RAIMUND OBER**

Professor, College of Medicine, Texas A&M University  
University of Southampton, UK

Exploring subcellular dynamics remains a major challenge. One of the main reasons is that the imaging of such events presents significant problems due to the extended depth of a cell. These problems are even worse when quantitation is required, such as in the three-dimensional tracking of single molecules. Here, the depth discrimination problem plays a major role. We will present our approach to address these problems using multi-focal plane microscopy and more recent developments. In multi-focal plane microscopy, several focal planes in a sample are simultaneously imaged, rather than sequentially, as is done in classical microscopy. We will illustrate our approaches with an example from the study of the subcellular trafficking pathways of antibody molecules.



---

---

# Abstracts

---

## LIFE SCIENCES Spring 2020

### **AEROALLERGENS OF THE TEXAS PANHANDLE, PARTICULATE MATTER 2.5 POLLUTION AND A NOVEL AIR PURIFICATION TECHNOLOGY AS A REMEDY. AUBREY HOWARD,<sup>1</sup> NABARUN GHOSH,<sup>1</sup> JEFF BENNERT<sup>2</sup> AND JON BENNERT<sup>2</sup>**

<sup>1</sup>Department of Life, Earth & Environmental Sciences, West Texas A&M University, Canyon, Texas 79015, <sup>2</sup>Air Oasis, Research and Development, 3401 Airway Blvd. Amarillo, Texas 79118.

For over two decades, we have analyzed the aeroallergen index of the Texas Panhandle to provide information on fluctuations regarding the onset, duration, and severity of the pollen season. Clinicians can use this information to guide allergen selection for skin testing and treatment. Fluorescence and Scanning Microscopy imaging are useful approaches to understand the structure and function of the microscopic objects. The aeroallergens are collected on a tape using a Burkard Volumetric Spore Trap (UK). The tape is stained with 2% Safranin and resulting prepared slides from the pollen are observed under an Olympus BX40 microscope equipped with FITC and TRITC fluorescent filters, a mercury lamp source, and an Olympus DP-70 digital camera connected to the computer with Image Pro 6.0 software. Aeroallergens are viewed, recorded and analyzed with DP Manager using the Image Pro 6.0 software. Micrographs are taken using bright field, the FITC filter, and the TRITC filter settings at 40X. A high-pressure mercury lamp or UV source is used to excite proteins that exhibit autofluorescence. Pollen grains were measured using imaging software to reveal information on the size of colpi or sulci and the distance between microstructures. The daily aeroallergen data on types and fluctuations of pollen and molds present in the area help in the diagnosis of allergy, asthma and respiratory illness. A recent growing concern on health is particulate pollution, also referred to as particulate matter (PM). The body has mechanisms to prevent inhalation of foreign substances in the air; however, particles that consist of a diameter of less than 10 micrometers are able to travel deep into the lungs and can enter the blood stream. This can have various adverse effects depending on the particles' composition and the amount and duration of the exposure. A research collaboration developed Advanced Hydrated Photo

Catalytic Oxidation (AHPCO®) and Bi-Polar ionization technology, which aims to reduce both indoor allergens and particulate matter, improving indoor air quality. Air Oasis is developing a new generation of air purifiers that utilize AHPCO® and Bi-Polar ionization technology, which produces a blanket of redundant oxidizers, targeting the particulate matters in the air and on surrounding surfaces to sanitize the air eventually. This novel air purification technology could be promising to decrease the incidence of allergic rhinitis, asthma and other more extensive lung conditions in the future.

### **A MICROSCOPIC CHARACTERIZATION AND SURVEY ON THE SPECIES OF PHYTO-PLANKTON OF THE TEXAS PANHANDLE. ANNA CENICEROS, BEATRIZ BURCIAGA, NABARUN GHOSH AND SANDY BABITZKE**

Department of Life, Earth & Environmental Sciences, West Texas A&M University, Canyon, Texas.

Phytoplankton consist of a diverse number of species found in freshwater ecosystems. One major component is Cyanobacteria. During photosynthesis, these primitive bacteria produce oxygen as they fix carbon dioxide dissolved in water. Cyanobacteria can produce taste-and-odor compounds, toxins, and noxious blooms. When there is a dense accumulation of Cyanobacterial cells within a water body, it results in algal bloom. Some algal blooms can release toxins that are harmful to animals and humans. In recent years, there have been reports of sickness and deaths of dogs in different parts of Texas. These animals became sick after swimming or taking a bath in water bodies infested with Cyanobacteria. There has also been evidence of fish killings (1). The fish died due to toxins produced by the algal bloom, specifically Cyanobacteria that produce cyanotoxin. The most common cause of fish kill is low dissolved oxygen. The result of human activities affects the amount of dissolved oxygen in the water. We collected samples from different water bodies in the Texas Panhandle. These areas included Ceta Canyon, Palo Duro Canyon State Park, Lake Meredith and Greenbelt Lake. The samples were collected using phytoplankton nets. The samples were placed in labeled containers. The containers were placed under light with their caps off to provide aeration. Slides were then prepared from samples. The slides were viewed under a BX-40 Olympus Digital Microscope attached to a DP-74 Digital Camera equipped with *CellSense* software to capture and analyze the micrographs at different magnifications. We also used Fluorescent Microscopy to analyze the chloroplasts

and cellular storage granules of the algal samples. Fluorescence Microscopy (FM) has become one of the most useful approaches to understanding the structure and function of the microscopic objects. When attached with a sophisticated digital microscopy system and imaging computer software, fluorescence allows us to study a wide variety of structures, storage materials, and metabolic procedures in different organisms. Epifluorescence and fluorescence microscopy are rapid and reliable tools for studying nitrogen fixing structures like akinetes and heterocysts (2, 3). The most common species of phytoplankton that were collected and observed under the microscope were *Anabaena variabilis*, *Euglena acus*, Pinnate Diatoms, *Volvox globator*, *Scenedesmus*, *Micrococcus*, *Gloeocapsa*, *Cladophora*, *Spirulina* and *Spirogyra* species; all showed fascinating characteristics revealed by fluorescence. Some structures in the organisms were visualized with the FITC filter and but not with the TRITC filter, and vice versa (4). The concentration of the phytoplankton collected from different areas was determined by using a Sedgewick-Rafter counter. The concentration and compositions of phytoplankton varied greatly from one area to another and based on the flow of water.

#### References:

1. Ghosh, N., Finger, K., Usnick, S., Rogers, W.J., Das, A. B. and Smith, D.W. (2010). Microscopic examination on cytological changes in *Allium cepa* and shift in phytoplankton population at different doses of Atrazine. *Scanning Microscopy 2010* (edited by Michael T. Postek, Dale E. Newbury, S. Frank Platek, David C. Joy.); SPIE Vol. 7729 Sec. W-1:1-14.
2. Scheirer, D.C. and Brasell, H.M. (1984) "Epifluorescence microscopy for nitrogen fixing blue green algae," *Am. J. of Botany*. 71:4:461-465.
3. Stephens, D. J. and Allan V. J. (2003) "Light Microscopy Techniques for Live Cell Imaging," *Science*. Vol. 300:5616:82-84.
4. Ghosh, N. and Whiteside, M. (2006) "Fluorescent Microscopy in Characterizing Some Biological Specimens," *Journal of Scanning Microscopies*, Vol. 28, No. 2 (March/ April 2006) 129-130.

#### UTILIZING MICROSCOPIC TECHNIQUES TO MONITOR DIFFERENTIAL INDUCTION OF MITOPHAGY AFTER EXPOSURE TO ENGINEERED ALUMINUM NANOPARTICLES. H. LUJAN, M.R. MULLENOS, and C. M. SAYES

Department of Environmental Science, Baylor University, Waco, TX

As advanced material processes utilizing metal nanoparticles continues to grow, nano-enabled products containing metal nanoparticles are becoming more widespread. One up and coming metallic nanomaterial being used for its wide range of beneficial properties is aluminum nanoparticles (AlNPs).

The possible toxicity for AlNPs, if any, have yet to be investigated. Toxicological assessments are warranted due to the known detrimental interactions of aluminum within mitochondria (i.e. respiration and ATP production.) Furthermore, metal nanoparticles have recently been studied for their propensity to trigger mitophagy, a process of mitochondrial specific degradation. Because of their size, tendency to generate ROS when suspended, and ability to interact with the mitochondria, we hypothesize that the AlNPs will elicit a profound dysregulation of mitochondrial health leading to mitophagy.

To determine the extent of mitochondrial dysregulation after exposure to AlNPs, three different types of human lung cells (i.e. cancerous, asthmatic, and normal primary) were characterized before and after exposure to a 1ppm concentration of AlNPs.

Multiple forms of microscopy were utilized to determine AlNP uptake, mitochondrial health, morphology, and presence of mitophagy. Darkfield hyperspectral imaging was used to determine the uptake of AlNPs into the cells. Transmission electron microscopy (TEM) techniques were utilized to visualize mitochondria and determine the size, size distribution, aspect ratio of mitochondria and other features unique to mitophagy were drawn from the TEM micrographs. Fluorescence microscopy and spectroscopic techniques were also employed to measure ROS levels.

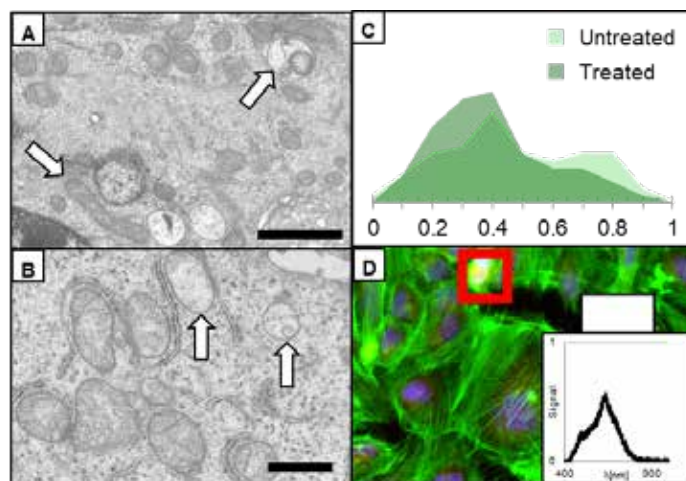


**Figure 1.** After exposure to AlNPs, mitochondria are seen to elongate, there is a production of autophagosomes (A) and cristae undergo degradation (B). The shift in average mitochondrial size is seen in (C) where untreated mitochondria are spherical and treated mitochondria are elongated. Uptake of AlNPs was confirmed with Hyperspectral Imaging (D).

Our data shows that mitochondrial dysregulation (i.e. average change in mitochondria size, shape and presence of autophagosomes) and more specifically mitophagy was more pronounced in the primary phenotype compared to the other two cell lines.

This methodology demonstrates novel Microscopic methods to determine small changes in mitochondrial health that has the potential to aid in the prediction of downstream adverse health outcomes after particle exposure. These findings will help guide future research using mitochondrial health as a biomarker or pathway for future research.

**SCANNING ELECTRON MICROGRAPHY OF THE STRUCTURE OF SECONDARY FLIGHT FEATHERS OF SINGLE COMB WHITE LEGHORN CHICKENS.** ISABELLA K. CARTER, JESSICA S. GONZALEZ Eastfield College, DCCCD, Mesquite, TX

This study is a continuation of research published by Dr. Alfred M. Lucas and Dr. Peter R. Stettenheim in *Avian Anatomy Integument Part 1* (1972). Their work describes the basic structure of feathers of the domestic fowl and was limited to observations using light microscopy. This project utilizes scanning electron microscopy (SEM) to further determine the structures of secondary male and female flight feathers. A Hitachi S-3400N SEM was used to provide more detailed images of the structures of vanes, barbules, and barbicels of secondary feathers. Electron micrographs were taken of the fourth secondary feather from a male and second secondary feather of a female. Structures were observed at different magnifications, providing higher resolution of the same structures using a light microscope. The scanning electron micrographs provided greater details of the structures of secondary flight feathers of SCWLCs and supported the findings described by Dr. Lucas and Dr. Stettenheim.

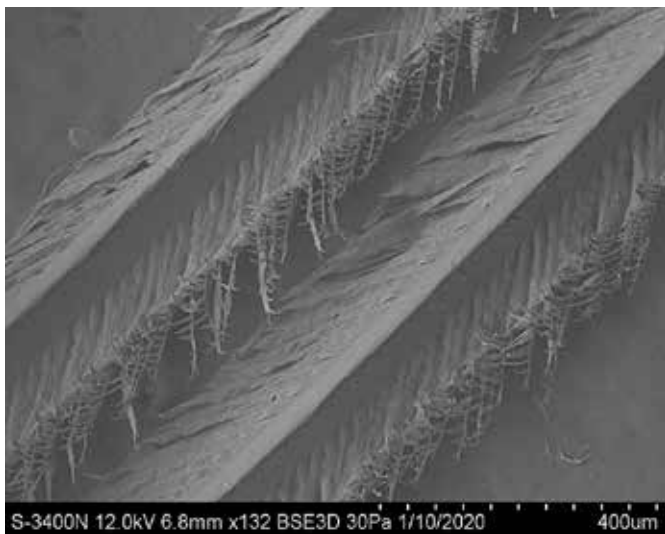


**Figure 1.** Female vanes, barbules, and barbicels of a secondary flight feather. Vanes are seen running in a straight line, while the barbules run from left to right. Barbicels appear as small hooks arising from the barbules.

**CIRCADIAN REGULATION OF SEROTONIN IN THE MOUSE GUT.** JULIET O. ELLISON and STEPHEN P. KARAGANIS

West Texas A&M University, Department of Life, Earth, and Environmental Sciences

In mammals, many physiological functions are controlled by circadian oscillators. A potential example is the production of serotonin within the gut, as levels circulating in the blood have been reported to vary throughout the day in some rodent species. Rhythmic production of serotonin in the gastrointestinal tract may be under the control of circadian oscillators. Understanding these mechanisms is important since dysregulation of serotonin is involved in the pathophysiology of numerous gastrointestinal disorders. This study examined how rhythmic environmental conditions of daily food availability or light exposure influences the mice's levels of serotonin and platelets circulating within the blood. C57BL/6 mice were housed in a 12:12 hour light:dark cycle at a constant temperature of 26°C. The control group had food *ad libitum*, with the experimental group's feed access restricted to a window of time during the day. Mice were maintained in these conditions for one week before sacrifice. Intestines, liver, blood, and fecal samples were collected and platelets counted using a hemocytometer every four hours over a 24-hour period. An ELISA of serum serotonin detected no rhythmicity in either group. Platelet counts were rhythmic in the restricted feeding group, but not in the *ad libitum* group.

**IDENTIFICATION OF A NEUROENDOCRINE INTERACTION UNDERLYING SEX DIFFERENCES IN TRIGEMINAL PAIN PROCESSING.** SUKHBIR KAUR and DAYNA L. AVERITT.

Texas Woman's University, Department of Biology, Denton, TX

Serotonin (5-Hydroxytryptamine, 5HT), a pain-generating component of the inflammatory response, activates and sensitizes sensory neurons of the peripheral nervous system. Our previous *in vivo* and *ex vivo* studies have shown that 5HT elicits pain via the excitatory 5HT<sub>2A</sub> and 5HT<sub>3</sub> receptors. In male rats, 5HT<sub>2A</sub> and 5HT<sub>3</sub> receptors are co-expressed on a subpopulation of sensory neurons that express *transient receptor potential vanilloid 1* (TRPV1) ion channels, detectors of noxious stimuli including capsaicin, heat, and protons. When sensitized by inflammatory mediators, TRPV1 activation results in increased transient calcium influx and post-synaptic release of proinflammatory calcitonin gene-related peptide (CGRP) leading to peripheral sensitization, thus, enhancing pain to protect the organism from further interaction with the noxious stimuli. These studies were conducted in male rats, so it is unknown whether this system is comparable in females. It is likely to be sexually dimorphic as a variety of pain disorders known to involve 5HT, such as irritable

bowel syndrome, migraine, and fibromyalgia, are more common in women. Further, it is unknown in either sex whether the effects of 5HT on TRPV1 are limited to potentiation or whether 5HT can directly sensitize TRPV1 to enhance pain. Of the pain disorders more common in women, craniofacial pain disorders, such as migraine and temporomandibular joint disorder, are the most common and have a 2-3X greater prevalence in women over men. Craniofacial pain disorders typically fluctuate with the menstrual cycle so it has been postulated that gonadal hormones, mainly estrogen (E2), modulate craniofacial pain mechanisms in women. Our recent data indicate that trigeminal pain is greatest when gonadal hormones are in flux and E2 enhances serotonergic potentiation of capsaicin-evoked CGRP release from rat trigeminal neurons, the sensory neurons specific to the craniofacial region. These data indicate a gonadal hormone-dependent interaction between excitatory 5HT receptors and TRPV1 on trigeminal sensory neurons. We hypothesized that *5HT<sub>2A</sub>* and/or *5HT<sub>3</sub>* receptor mRNA is co-expressed with *TRPV1* mRNA in female trigeminal sensory neurons and that the additional presence of E2 at the sensory neurons enhances 5HT potentiation of TRPV1 activity.

Trigeminal ganglia were extracted from adult cycling female rats at each stage of the estrous cycle (analogous to the human menstrual cycle). Ganglia were frozen, sectioned at 30  $\mu\text{m}$ , and mounted on slides. Slides were then processed for *in situ* hybridization using RNA oligo probes designed against *5HT<sub>2A</sub>*, *5HT<sub>3</sub>*, and *TRPV1* mRNA, according to the manufacturer's protocol (ACD Biotechnie RNAscope®). Images were obtained using a Nikon Eclipse Ti Swept-field/STORM confocal microscope. Trigeminal ganglia were extracted from a separate group of ovariectomized female rats and cultured for 5 days in 96-well plates. Neurons were pretreated for 30 mins with 50 nM E2, incubated with Fluo-4 AM dye, then treated with a combination of 50  $\mu\text{M}$  5HT and 5, 10, 20, or 30 nM capsaicin. Calcium influx during each treatment was captured and quantified using a Biotek Cytation 5 plate reader. Cells were then fixed in 4% paraformaldehyde and processed with immunohistochemistry to visualize estrogen receptor and TRPV1 protein expression. All data was analyzed using Graphpad Prism 8.3, Nikon Elements AR Analysis, and NIH Image J software.

Fluorescent punctate expression was observed with the high, medium, and low expressing positive control probes in our trigeminal ganglia cells. This expression was not observed in slides treated with the negative control probes. Further, tissue collection method (dry ice vs liquid nitrogen) or tissue storage time (1-week vs 2 years) did not differentially affect the probe binding and signal intensity. We are currently analyzing the expression of *5HT<sub>2A</sub>*, *5HT<sub>3</sub>*, and *TRPV1* mRNA. In trigeminal neuron cultures, capsaicin and 5HT elicited a concentration-dependent calcium influx. Further, our

preliminary data indicate that pretreatment with E2 enhanced 5HT-evoked calcium influx and the pattern of influx is indicative of TRPV1 desensitization. Overall, this work aims to locate the anatomical substrate for the sexually dimorphic effects of inflammatory mediators on trigeminal pain processing.

## **PARTICULATE MATTER 2.5 POLLUTION AND THE NEED FOR AIR PURIFICATION TECHNOLOGY.**

HERLINDA LEE,<sup>1</sup> TASIA BOS,<sup>1\*</sup> NABARUN GHOSH,<sup>1</sup> JEFF BENNERT<sup>2</sup> and JEREMIAH DORSETT<sup>2</sup>

<sup>1</sup>Department of Life, Earth & Environmental Sciences, West Texas A&M University, Canyon, Texas 79015, <sup>2</sup>Air Oasis, Research and Development, 3401 Airway Blvd. Amarillo, Texas 79118.

Allergies, asthma and hospitalizations for respiratory diseases are rising worldwide due to air pollution with aerosols in the form of Particulate Matter 2.5 (PM 2.5), in addition to other aeroallergens. The PM 2.5 is largely responsible for air pollution all over the world, which leads to serious health hazards and death because of its size. Studies on improvement of outdoor air quality are extremely important for everyone's health. There are many reports of poor air quality, with measurements above the prescribed safe level, in Beijing (China), Delhi (India), Istanbul (Turkey), Hanoi (Vietnam), in Southeastern Brazil, in Los Angeles and New York (U.S.A.) In some locations like Beijing, wearing a mask during commutes is common practice because of high PM 2.5 concentration. Advances have been made in the air purification system, including the development of the Advanced Hydrated Photocatalytic Oxidation (AHPCO) and Plasma-technology used in the unit called i-Adapt, by Air Oasis in Amarillo, Texas. This technology aims to improve the indoor air quality, specifically targeting PM 2.5 and various other aeroallergens. The unit was tested to evaluate its performance in removing PM 2.5 within a fiberglass chamber. In this experiment, we used dust containing Particulate Matters (PM) with an average size of 2.75micrometers (ISO 12103-1 Ultrafine Dust Particle, PTI Powder Tech., Minnesota) in order to measure particle concentration. The i-Adapt unit was placed inside a fiberglass chamber to exert its effects on the circulating dust. We measured the natural rate of decay and compared that of the i-Adapt unit, to assess the proficiency of this newly developed air purification unit. After the fans ran for 24 hours, the i-Adapt unit was turned on, and readings of PM 2.5, reflecting air quality, were taken at 24, 72, and 120 hours using a Temtop M2000C air quality meter. The average PM 2.5 count was 51.2  $\mu\text{g}/\text{m}^3$  after spreading and saturating the air in the chamber using four fans in the corners of the fiberglass chamber. The count went down to 17 after the first 24 hours on running the i-Adapt air purifier. The PM 2.5 counts were down to 9.3  $\mu\text{g}/\text{m}^3$  and 4.3  $\mu\text{g}/\text{m}^3$  after 72 and 120 hours of running the unit. The

gradual reduction of the PM 2.5 count revealed the high efficiency of the i-Adapt air purifier. Further studies should be conducted to establish the applications of the i-Adapt unit to the various facets of our lives.

*\*\*McNair Scholar, This Project was funded by the McNair's Scholarship, 2019.*

**THE COLORADO TICK FEVER VIRUS INDUCES NF-KB AND HMGB1 ACTIVATION IN THE HUMAN MICROVASCULAR ENDOTHELIAL CELL LINE HMEC-1. LUIS GRADO, RAJESH BALARAMAN, and JEREMY BECHELLI**

Department of Biological Sciences, Sam Houston State University, Huntsville, TX

Colorado tick fever virus (CTFV), the causative agent of Colorado tick fever (CTF), is a segmented, double-stranded RNA virus, in the *Coltivirus* genus and the *Reoviridae* family. CTF is generally a mild and self-limiting disease characterized by biphasic fever, headache, myalgia, fatigue and, a petechial rash. However, children can develop a more severe illness leading to meningitis, encephalitis, hemorrhagic fever, and death. There is little information on the mechanisms underlying CTFV induced pathology and severe complications during infection. Our current work has shown that CTFV induces apoptosis and caspase-3/7 activation in human microvascular endothelial cells (HMEC-1). Examples in the literature show that reoviruses activate transcription factor nuclear factor kappa B (NF-kB), which exerts a pro- rather than antiapoptotic phenotype. Additionally, NF-kB activation can result in the release of high mobility group box 1 (HMGB1), a pro-inflammatory cytokine, released in response to injury or infection. To identify host cell factors that mediate apoptosis and inflammation in human endothelial cells, we investigated whether CTFV infection alters the activation state of NF-kB and the secretion of high-mobility group box-1 (HMGB1) using confocal laser scanning microscopy. In cells infected with CTFV for 24 hours, we demonstrate that CTFV activates caspase-3/7 activation and that RelA translocates from the cytoplasm to the nucleus, which is indicative of NF-kB activation. Furthermore, cells infected with CTFV show a potent translocation of HMGB1 from the nucleus into the cytoplasm. Our experimental data suggest that CTFV activates caspase-3/7, induces NF-kB activation, and HMGB1, which may contribute to disease progression during CTF.

**DIFFERENTIATING RESPIRABLE SENSITIZERS AND IRRITANTS USING *IN VITRO* MODELS: ANALYSIS OF CELL-BASED MONOLAYERS VERSUS CO-CULTURES. MATTHEW GIBB and CHRISTIE M. SAYES**

Department of Environmental Science, Baylor University, Waco, TX

In an effort to decrease the use of animals in toxicological research testing, investigations that lead to verifiable *in vitro* testing methods are desperately needed. Unlike the skin, lungs lack validated and universally-accepted *in vitro* testing methods that differentiate between irritating and sensitizing aerosols. To complicate the issue further, these toxicity-inducing aerosols could exist as either liquid droplets or solid particulates. Therefore, validating an *in vitro* model requires both comprehensive aerosol and cell characterization. Previously, we have developed and tested an *in situ* real-time model system that collects both physical, chemical, and biological data before, during, and after aerosol exposure to lung cell cultures at the air-liquid interface. In this study, we further investigate *in vitro*-based testing systems by utilizing the liquid-liquid interface to compare the irritation versus sensitization effects to cell monolayers and co-cultures of pulmonary cells. The monolayer includes human lung epithelial cells, only; while the co-culture consists of epithelial cells plus human monocytes transformed into macrophage-like phenotype and dendritic cells that function as antigen presenting cells. Fluorescence and electron microscopy were utilized to investigate ultrastructure and morphology before and after exposure. Results show that after exposure to the known solid particulate irritant crystalline silica nanoparticles, the co-culture model produced significantly more TNF-alpha as compared to the monolayer, suggesting the importance of using multiple cell-types when validating *in vitro* models. Similar results were found when exposing the known sensitizer nickel oxide and subsequently measuring endpoint IL-13. Interestingly, particle silver colloids did not induce a measurable increase in either biomarker (when compared to untreated control cell populations). These results show that *in vitro* co-culture models may be suitable for initial screening assessments of new materials suspected as either irritants or sensitizers. Implementation of this model would aid in the acceleration of bringing newly developed products (and formulations) in the laboratory to the commercial market.

**ENHANCING VISUALIZATION OF MORPHOLOGICAL CHARACTERISTICS OF *ESCHERICHIA COLI*, *STAPHYLOCOCCUS AUREUS*, AND *CORYNEBACTERIUM XEROSIS* THROUGH THE APPLICATION OF IONIC LIQUID. MONICA I. PIÑON GALVAN, CHRISTIEN CARTER, JESSICA S. GONZALEZ.**

Eastfield College, DCCCD, Mesquite, TX

The procedures and techniques used to prepare specimens in scanning electron microscopy (SEM) are critical, as they affect the quality of the images. Bacteria present an even greater challenge because of size, fragility, and the charge they emit. The beam and vacuum of the SEM has a negative effect on biological specimens causing them to dehydrate, shrivel up, and

emit a large amount of charge. Furthermore, the SEM is a less common instrument used to study bacteria; transmission electron microscopy (TEM) being the standard. In this experiment a 5% Ionic liquid (Hitachi HILEM IL1000) solution was used to float TEM grids each with one of the following bacterial species: *Escherichia coli*, *Staphylococcus aureus*, and *Corynebacterium xerosis*. The aim was to reduce dehydration and charge of the organisms, to produce high quality images. Inocula from each of the three species were grown on tryptic soy agar (TSA) plates, transferred onto a TEM copper grid, and viewed under a Hitachi SEM S-3400N. Each specimen was also imaged without ionic liquid and served as controls. Bacteria without IL1000 showed cracks, evidence of dehydration, and emitted great amounts of charge interfering with the quality of the images. Bacteria with IL1000 had no sign of charge or dehydration, resulting in improved visualization of the organisms and higher quality images of morphological structures and arrangement. The images acquired throughout the experiment, with and without ionic liquid, were compared. IL1000 resulted in improved image quality, keeping the bacterial specimens hydrated with little or no charge.

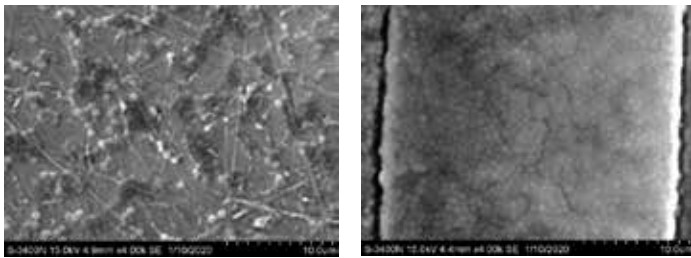


**Figure 1. A.** *Staphylococcus aureus* imaged at 15.0kV, a working distance of 4.9mm, and at x4.00k magnification. Placed on a TEM copper grid and floated on a 5% Hitachi HILEM IL 1000 solution for 30 min then rinsed twice with deionized water. **B.** *Staphylococcus aureus* imaged at 15.0kV, a working distance of 4.4mm, and at x4.97k magnification, placed on a TEM copper grid without 5% Hitachi HILEM IL 1000 solution and imaged. \*All micrographs were taken using a Hitachi S3400N SEM. Scale bar = 10 um.

**EMULATION OF SPIDER WEB SPINNING PROCESS.** RODERICK L. KINES<sup>1</sup>, ELIJAH RAY MARTINEZ<sup>2</sup>, MARK A. TURNER<sup>1</sup>, and JESSICA S. GONZALEZ<sup>1</sup>  
<sup>1</sup>Eastfield College, DCCCD, Mesquite, TX; <sup>2</sup>University of North Texas at Dallas

In 1962, Stan Lee and artist Steve Ditko created one of the most famous Marvel characters to ever grace the pages in the graphic novel *Amazing fantasy # 15*. That character was the *Amazing Spider-Man*, whom of which is the inspiration for this project. Spider-man's signature abilities are wall-crawling, proportionate strength, speed of a spider, and web spinning via twin devices worn on his wrists. The web spinner project was created to mimic a biological phenomenon that occurs naturally in spiders,

moths, and caterpillars which is web/silk spinning. The goal is to determine whether a mechanical device could be created in resemblance of Spider-Man's web shooter and preform the same web spinning capabilities of a spider. Utilization of the scanning electron microscope (SEM) allowed for accurate 3D printing of a prosthesis that models the spinneret of a spider. This spinneret is comprised of multiple microscopic extrusion ports that come to a fine follicle-like point. The web spinner incorporated this anatomical concept into its design due to its vital role in the spinning process. This spinneret is designed to fit onto the extrusion end of a 12V solenoid valve. This solenoid is the pathway between the web spinners pressure/fluid source and the open environment. This is all actuated by an Arduino nano which operates as the brain of the circuit. This brain is then given a signal from a NO (normally open) push button. This normally open state means the button will not constantly send false signals to the Arduino, which would then cause undesired firing. The key components of the web spinner's circuit are modeled after the process a spider goes through during silk spinning; the SEM allowed detailed visualization of the spinneret itself. In conclusion, the combination of electrical/mechanical engineering and microscopy allowed the web spinner to accurately model an actual silk spinning spider.

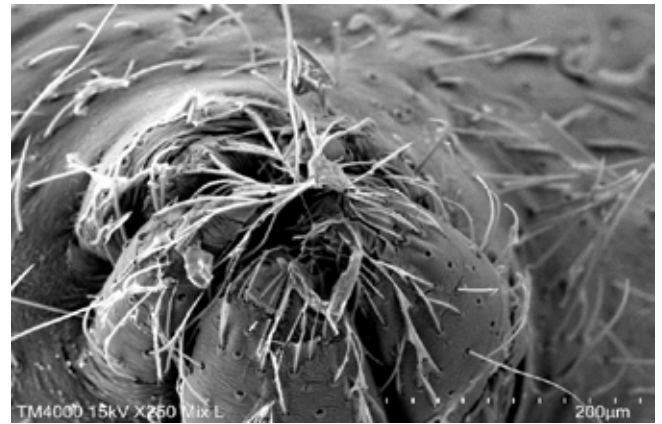


**Figure 1.** SEM image of a common house-hold spider's spinneret after just spinning a web.

**6-HYDROXIDOPAMINE (6-ODHA) INDUCED TOXICITY ON *IN VITRO* NEURONAL AND GLIAL CELL MODELS.** SAHAR H. PRADHAN and CHRISTIE M. SAYES

Department of Environmental Science, Baylor University  
 Parkinson's disease (PD) is a neurodegenerative disorder, which exhibits the preferential loss of dopaminergic neurons in the substantia nigra pars compacta (SNpc), this dopaminergic loss results in clinical motor symptoms such as rigidity, bradykinesia and the characteristic resting tremor. *In vivo* and *in vitro* models have helped to elucidate mechanisms for Parkinson's disease, using neurotoxins such as

6-hydroxydopamine (6-ODHA) or MPTP+, which mimic the biochemical and histological characteristics of PD. Mechanisms behind 6-ODHA induced PD, focuses on oxidative stress and mitochondrial defects, both of these are led by increased ROS generation, of which nigral cells are especially vulnerable due to the lack of synthesis of glutathione peroxidase in the SNpc. *In vitro* models, to characterize PD, often utilize either a glial cell model or a neuronal cell model, these two approaches help in elucidating an inflammatory and neuronal characterization. For this present study, Normal Human Astrocytes (NHAs), differentiated and undifferentiated SH-SY5Y neuroblastomas were used in an exposure with 6-ODHA. Astrocytes are a significant part of this model because they are not well characterized in the literature and in terms of the GABAergic pathways, astrocytes account for glutamine (precursor for glutamate) and GABA efferent into neurons. Proliferation, whole cell analysis, metabolic quantification and gene expression was measured for pre- and post-treatment, fluorescence and electron microscopy was used to indicate points of mitochondrial stress or damage. Results indicate that treatment with 6-ODHA leads to an oxidative stress pathway beginning with autooxidation, followed by increased ROS generation and eventual apoptosis, ROS was indicated through Confocal Laser Scanning Microscopy (CLSM). In terms of mitochondrial dysfunction, 6-ODHA directly targets the electron transport chain through the inhibition of complex I and reduces ATP production indicating apoptosis, mitochondria were imaged using Transmission Electron Microscopy (TEM). 6-ODHA toxicity is specific, in that it directly affects dopamine (DA) by acting on dopamine transporters (DAT), and indirectly reduces glutamate expression through astrocytic apoptosis by the activation of inflammatory pathways. The impact of these results is furthering the characterization of glial cells in PD models, as well as mitochondrial dysfunction, as more specific mechanism for PD. In addition, this study shows the use of microscopy to elucidate mitochondrial damage on neuronal cell types.

#### **TAXONOMIC IDENTIFICATION OF AN EAST TEXAS MIOCENE PROBOSCIDEAN IVORY TUSK FRAGMENT. SAVANAH DAVIS, PATRICK LEWIS and RAJESH BALARAMAN**

Sam Houston State University, 3161 Clay Circle, Huntsville, TX 77340

The goal of this project was to identify a proboscidean tusk fragment found in Rush Creek (near Woodville, Texas) down to genus. Since ivory microstructure is a diagnostic for many proboscideans, scanning electron microscopy (SEM) was used to study the microstructure of ivory. Microstructural features of the ivory examined included dentinal tubules, dentinal ridge presence, and overall texture (smooth/rough, distribution of tubules).

Contradictory of most SEM samples, ivory does not require chemical preparation that can be detrimental to fossils. This project is relevant, for it could allow new conceptualizations of the paleoecological environment. If using this technique provides a new faunal distribution, the estimated knowledge of the paleoecological environmental information would need to be updated to include the genus and its possible impact. The method used in this study is courtesy of Lambert (1) but has been updated with use of Varied Pressure-SEM (VP-SEM). It was found during imaging that utilizing VP-SEM mode in lieu of normal SEM mode produced higher resolution images. VP-SEM allows for biological samples that contain moisture to be imaged topographically in high resolution with a large depth of field. Comparatively, Lambert imaged using normal SEM mode and magnifications 300X, 1000X, and 1500X. In this study, images were obtained at these magnifications, and also 3000X. Overall, the genus of the sample was conclusively found to be *Gomphotherium*. After completing this identification, a continuation of SEM imaging of ivory is planned, in which several assorted samples of fossilized ivory are to be imaged and identified using VP- SEM.

#### **References**

1. Lambert, W.D. (2005). The microstructure of proboscidean ivory and its application to the subordinal identification of isolated ivory specimens. *Bull.Fla.Mus.Nat.Hist.*, 45(4): 521-530.

#### **GASTROINTESTINAL ENDOSCOPY FOR MANIFESTATION OF HOOKWORM. PRABIR KUMAR BANERJEE<sup>1</sup>, SHATAVISA MUKHERJEE<sup>2</sup>, SHAILY GOYAL<sup>3</sup> and NABARUN GHOSH<sup>3</sup>**

<sup>1</sup>RN. Tagore International Institute of Cardiac Sciences, Kolkata, India. <sup>2</sup>School of Tropical Medicine, Kolkata, India; <sup>3</sup>Life, Earth and Environmental Science, West Texas A&M University, Canyon, Texas.

Hookworm infestation is quite common in tropical countries. It is responsible for gastrointestinal (GI) bleeding and iron-deficiency anemia (1). According to the Global Burden of Disease Study (2), hookworms affect approximately 500 million people, with 5.1 billion at risk for acquiring infection worldwide (3). Hookworm infestation is predominantly due to two human-specific nematodes: *Ancylostoma duodenale* and *Necator americanus*, distinguished from each other by the morphological differences of their mouth capsules, bursae and spicules. The infestation is related to poor hygiene. It can even be acquired by walking barefoot on soil contaminated with infected human feces. Infection onset occurs when filiform larvae penetrate the human skin, migrate into the circulation, and reach the pulmonary alveoli and trachea. Infection can also occur by ingestion, as in the case of *A. duodenale*. Most infected individuals are asymptomatic, while the

symptomatic clinical manifestations include pulmonary eosinophilia, iron- deficiency anemia, and occasionally cutaneous larva migrans. Usually, the diagnosis is made by the characteristic clinical findings, eosinophilia and egg appearance on fecal examination (4). However, diagnosis is often missed due to the absence of eggs in stool or eosinophilia. Upper GI endoscopy (Esophago-Gastro-Duodenoscopy) appears to be an important imaging tool for the diagnosis of gastrointestinal problems, and is often used for Hookworm diagnosis. If present, these parasites usually live in the upper part of the small intestine but relatively few in the duodenum. Recently, wireless capsule endoscopy (WCE) has been used for automatic hookworm detection. Unfortunately, it remains a challenging task (5). In the present study, we detected the presence of Hookworm by routine GI endoscopy, as shown in the Figure 1. The study was carried out from September 2017 to October 2019 in the rural and sub-urban areas of West Bengal, India. It included referral patients from age group of 20 to 50 years. Patients were mainly farmers. 3,300-3,500 procedures of upper GI endoscopy were done per year. An average of 0.5 to 1 case of *A. duodenale* was observed per month. 1-3 cases of obscure gastrointestinal bleed were documented per year. Few of such cases are detailed below. Case-1: A 40 years old male presented with abdominal pain, dizziness, dyspnea and palpitation on excursion the past 3 months, with occasional history of blackish stool. The patient had conjunctival pallor with regular heart rate (100 bpm), and laboratory findings of eosinophilia, Hb-8 g/dl, PCV-24.5%, MCV-68 fl, MCH-20 pg, MCHC-22 g/dl, RDW-18%; Serum Cr-0.9 mg/dl and Serum Ferritin-10 ng/ml. Stool examination did not show any eggs or parasites. Electrocardiography found sinus tachycardia, while ultrasonography (USG) of the abdomen was unremarkable. In 6 weeks, the patient was given four units of blood and was managed with Albendazole (antihelminth) and oral iron therapy after endoscopic diagnosis. Case-2: A 32-year-old female presented with anorexia, bloating, and pica (geophagia) for the past 6 months. Remarkable conjunctival pallor was observed. The urine pregnancy test was negative. Craving for soil compounds (geophagia) occurs in both Iron deficiency anemia (IDA) and pregnancy. Clinical findings included Hemoglobin-9 g/dl, PCV-27.8%, MCV-70 fl, MCH-22 pg, MCHC-24 g/dl, RDW-17%, Serum Ferritin- 25 ng/ml. Serum creatinine-1mg/dl. She received two units of packed RBC and was treated with Albendazole and iron tablets. Case-3: A 21 years old male presented with bloating, anorexia and abdominal pain on food intake for 1 month. The patient had epigastric tenderness with questionable conjunctival pallor. Laboratory investigations yielded Hb-12 g/dl, PCV- 37%, MCV-78 fl, MCH-26 pg, MCHC-32 g/dl, and RDW-14.6%. The serum creatinine was 1mg/dl, while serum ferritin – 105 ng/ml. Hemoglobin electrophoresis was normal, along with unremarkable

ultrasonography of the abdomen. In all of the above cases, upper GI endoscopic findings were unremarkable with no ulceration, tumor, abnormal vessels, structure or deformity but revealed presence of duodenal hookworm (*Ancylostoma duodenale*) (Figure1). Parasite infections should always be considered as a differential diagnosis in patients with iron-deficiency anemia and unexplained or obscured gastrointestinal blood loss, especially in poor sanitary set-ups. Careful observation up to distal duodenum, in upper GI endoscopy is necessary. As in the above cases, close examination helped in diagnosing Hookworm infestation with or without any pointer including stool examination or eosinophilia. Hookworm infestation is a treatable condition where treatment involves use of mainly benzimidazole drugs like mebendazole and albendazole, which act by inhibiting microtubule polymerization in invertebrates, thus killing the adult worms. Three consecutive daily doses of either drug is an effective treatment protocol. Being a soil transmitted disease, improved sanitation and hygiene plays a vital role. Community awareness in this regard is highly warranted.



**Figure 1.** Hookworms attached to duodenal mucosa and blood oozing.

#### References:

1. Wei, KY., Q. Yan, B. Tang, B., et al. (2017). Hookworm Infection: A Neglected Cause of Overt Obscure Gastrointestinal Bleeding. *Korean J. Parasitol.* 55:391–398.
2. Global Burden of Disease Study (2013) Collaborators. 2015. Global, regional, and national incidence, prevalence, and years lived with disability for 301 acute and chronic diseases and injuries in 188 countries, 1990–2013: a systematic analysis for the Global Burden of Disease Study 2013. *Lancet* 386:743–800. 10.1016/S0140-6736(15)60692-4.
3. Pullan, R.L., S.J. Brooker. (2012). The global limits and population at risk of soil-transmitted helminth infections in 2010. *Parasites & Vectors* 5:81.
4. Tomoda Y, T. Chaen, K. Sakai, K. Tanaka (2019) Abdominal pain and hookworm infection. *QJM: An International Journal of Medicine*,1-1.doi: 10.1093/qjmed/hcz276

5. Wenju, D.U., N. Rao, D. Liu, H. Jiang, C. Luo, Z. Li, T. Gan, B. Zeng. (2019). "Review on the Applications of Deep Learning in the Analysis of Gastrointestinal Endoscopy Images", Access IEEE, vol. 7, pp. 142053- 142069.

**MICROSCOPY OF COLLAGEN PRODUCTION IN CHONDROCYTES.** SOUMILEE CHAUDHURI, PRIYANKA BRAHMACHARY, and RONALD JUNE

Department of Microbiology & Immunology and Department of Mechanical & Industrial Engineering, Montana State University, Bozeman, Montana-59717.

Chondrocytes function by regulating extracellular matrix turnover and maintaining tissue homeostasis in bones (1). Disruption of their function has been implicated in prognosis of articular degenerative diseases such as osteoarthritis. Ongoing tissue engineering approaches rely heavily on the impact of ascorbate in the regeneration of cartilage integrity. Imaging of ascorbate-supplemented collagen synthesis is instrumental in evaluating and devising strategies for therapeutic intervention in case of such arthropathies. In this context, the goal of this ongoing project was to look at ascorbate-dependent collagen production in chondrocytes. For microscopic analysis, primary chondrocytes grown as a monolayer in 50mg/ml ascorbate for 10 days, and then stained for collagen VI (Anti-Collagen VI antibody, ab6588 from Abcam), nuclei (Vibrant Blue) and mitochondria (Mitotracker). Control cells were not grown with ascorbate. Images were acquired on a Leica TCS SP8 confocal microscope with a 63x objective.

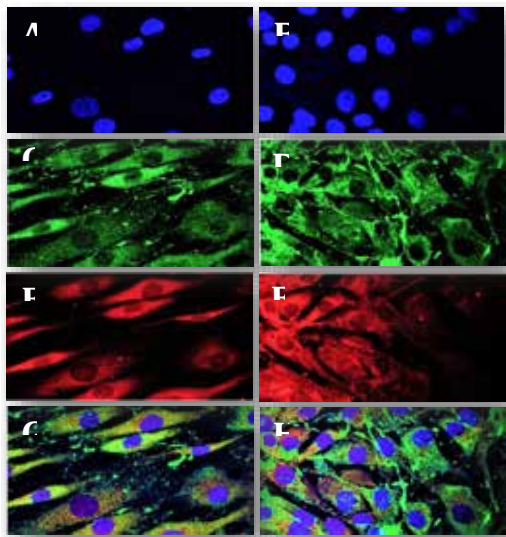


**Figure 1.** Ascorbate promotes collagen accumulation in chondrocytes. Cell monolayers were grown in the presence (right panels) or absence (left panels) of ascorbate. Nuclei (A, B), collagen (C, D), and mitochondria (E, F) were imaged after staining with Vibrant DyeCycle, Anti-Collagen VI antibody, and MitoTracker CMXRos, respectively. Merged images for each experimental setting are shown in panels G and H. Photomicrographs were acquired with a Leica TCS SP8 laser scanning confocal microscope.

**References**

1. Akkiraju, H., & Nohe, A. (2015). Role of Chondrocytes in Cartilage Formation, Progression of Osteoarthritis and Cartilage Regeneration. *Journal of Developmental Biology*, 3(4), 177–192. doi: 10.3390/jdb3040177

**THE MICROSCOPIC ANATOMY OF DWARF GECKO (GENUS SPHAERODACTYLUS) TOE-PAD SETAE USING SEM IMAGES.** ZILDJIAN BROOKS, RAJESH BALARAMAN, and JUAN DIEGO DAZA

Sam Houston State University, Department of Biological Sciences, Huntsville, TX, 77340.

Only three lizard groups have developed scansoriality by means of toe pads (skinks, iguanians and geckos). Geckos have developed this trait multiple times, and in any case their toe-pads consist of lamellae, which are formed by microscopic keratinous hairs known as setae. Combination of van der Waals forces and electric charges have been proposed to explain toe-pad adhesion, and variation in toepad morphology, size, shape and overall number of setae might explain differences in surface density among scansorial lizards. Toe-pads have been studied in multiple genera, and yet have only been briefly investigated among dwarf geckos (genus *Sphaerodactylus*), the smallest amniotes in the world. Here we studied seven species from the Puerto Rican Bank suggesting that there are noticeable morphological differences in the size of setae among species. There are also differences in the ratio between setae and body size when compared to other genera. This variation could be used as morphological features that might play some role in ecomorphological differentiation among geckos dwelling in different microhabitats in this insular area.

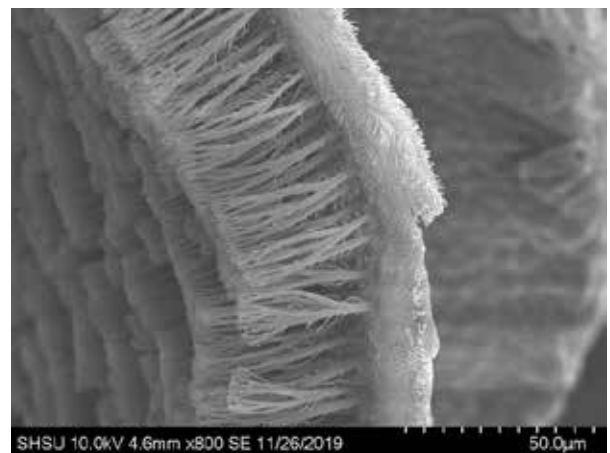


**Figure 1:** *S. roosevelti* setae imaged using SEM.

**ELECTRON TOMOGRAPHY AND SERIAL BLOCK SCANNING ELECTRON MICROSCOPY REVEAL THERAPEUTIC EFFECTS OF THE GOLD NANOPARTICLES AGAINST BREAST CANCER CELLS.** ANINDITO SEN<sup>1</sup>, SREEJITH RAVEENDRAN<sup>2</sup>, HIROMI ITO-TANAKA<sup>3</sup>, KAZUNORI KATO<sup>3</sup>, TORU MAEKAWA<sup>2</sup>, and D. SAKTHI KUMAR<sup>2</sup>

<sup>1</sup>Microscopy and Imaging Center, Texas A&M University, 301 Old Main Dr., College Station, TX 77843-2257, U.S.A; <sup>2</sup>Bio-Nano Electronics Research Center, Graduate School of Interdisciplinary New Science, Toyo University, 2100, Kujirai, Kawagoe, Saitama 350-8585, Japan; <sup>3</sup>Department of Biomedical Engineering, Research Centre for BME, Toyo University, 2100, Kujirai, Kawagoe, Saitama 350-8585, Japan.

Breast cancer is one of the most dreadful diseases the human civilization suffers from. In spite of surgical resections and combinatorial chemoradiations, some highly malignant populations of tumor cells revitalize, metastasize, and even develop inherent chemoresistance. Recent research has shown significantly favorable results in cancer cell killing by induction of apoptosis/necrosis by employing Therapeutic gold Nanoparticle (TAN), which is an amalgamation of gold nanocages (AuNcg) (Figure 1 inset) coated with mauran (MR) polysaccharide, functionalized with 4-hydroxytamoxifen (4OHT) and anti-TROP-2 monoclonal antibodies (MAb).

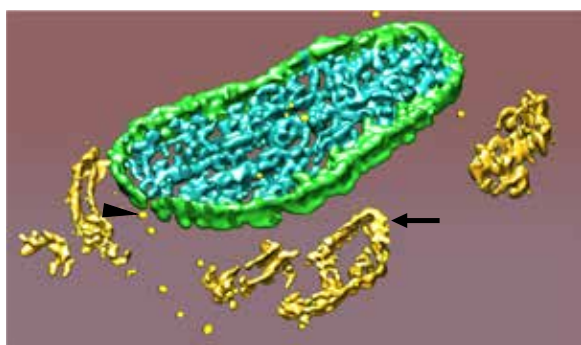


**Figure 1.** Three-dimensional (3D) map of a mitochondrion surrounded by ER and TAN (pointed by the black arrowhead). Just next the arrowhead is the rupture of the mitochondrial outer membrane due to TAN toxicity. The black arrow points to damaged smooth Endoplasmic Reticulum. Inset: SEM image of AuNcg showing corner truncations (green arrows).

Electron Tomography (ET) and Serial Block Face Scanning Electron Microscopy (SBF-SEM) studies on the association of TANs with the MCF breast cancer cells revealed a specific sequential process of disintegration of mitochondrial components in the diseased cells, due to the toxicity delivered by TANs. This leads to mitophagy, a process

in which damaged or non-functional mitochondria form autophagosomes. The results indicate that the mitochondrial membranes are ruptured by the TANs generating multiple fissures (Figure 1). Other TANs access the interior of the mitochondrion through these fissures, destroying the matrix and lamella, thereby leading to apoptosis and necrosis. ET of TAN damaged smooth Endoplasmic Reticulum (ER) (black arrow in Figure 1), develop Isolation Membranes (IM), which initiates the autophagy pathway. Simultaneous damage to the ER, mitochondria and lysosomes lead to type I and/or type II cell death in cancer cells.

**HYPERSPECTRAL IMAGING TO ELUCIDATE THE CHARGE DEPENDENT - UPTAKE OF SILVER NANOPARTICLES IN HUMAN LIVER CELLS.** MARINA R. MULENOS and CHRISTIE M. SAYES

Department of Environmental Science, Baylor University, Waco TX, 76706

With recent technological advances in hyperspectral imaging, a corresponding interest in cellular uptake of nanoparticles has increased. Previously in the literature, transmission electron microscopy (TEM) was used to monitor where nanoparticles accumulate in the cell. However, this technique is labor intensive and not cost efficient for the general lab. Hyperspectral imaging is user friendly, cost effective, and the sample preparation is less labor-intensive compared to TEM. Many studies in the literature show that nanoparticles of different composition, charge, or morphologies can accumulate in different parts of the cell, but these studies have been limited to engineered particles. There is an increasing need to investigate where biologically transformed nanomaterials will accumulate inside tissues and cells. Here, we studied biotransformed silver nanoparticles (AgNPs) of either positive, negative, or neutral charge. Each particle system was incubated in different physiologically-relevant environments: acidic stomach fluid, neutral blood serum, and basic surfactant fluid. Human hepatoma cells, HepG2, were exposed to the particles for 24 hours and analyzed with hyperspectral imaging (Figure 1). Our results indicate that the particles which released ions had an increase in cell penetration. The surface charge directly influenced the uptake mechanism in which the transformed particles entered the cell, and additionally provided evidence that the stomach-digested silver nanoparticles undergo dissolution in cytosolic vesicles. The spectral maps were significantly different from each other due to charge variation. Furthermore, the concentration of silver uptake into the cell was quantified via ICP-MS methods where the digested particles were seen to have the largest concentration of particle, or produced particle ions in the cell. The information obtained from these studies provides crucial insight into colloidal stability of nanoparticles, provides read-across comparisons between engineered and transformed

metal-based particles, and aids in filling the literature gap determining how colloidal stability affects to nanoparticle biotransformation, *in situ*.

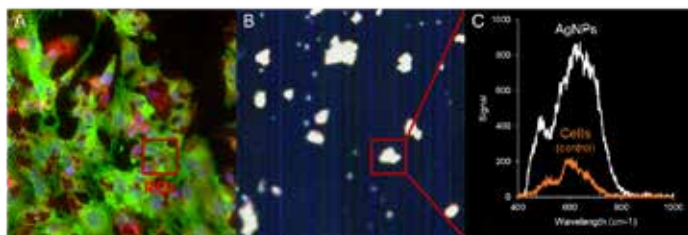


**Figure 1.** Fluorescent microscopy (A) was used as a supplementary technique to determine the region of interest for the hyperspectral imaging (B). Green represents cytoskeleton, blue represents nuclei, and red represents mitochondria. A spectrum was taken at the region of interest (C) and protein coated-silver nanoparticles were identified.

**VERTICAL STACKING OF ELECTRODEPOSITED NANORODS WITH CONTROLLED DIMENSIONS AND CHEMICAL COMPOSITION.** ARTURO GALINDO, JOSE LUIS REYES, AND ARTURO PONCE  
Department of Physics and Astronomy, University of Texas at San Antonio, San Antonio, TX.

We have developed a method designed to assemble vertical layers composed of ultra-dense arrays (1Tb/inch<sup>2</sup>) of Ni and Co nanorods. The fabrication scheme allows total control of the nanorod's dimensions (diameter and length) by using porous anodic aluminum oxide (AAO) membranes. A two-step anodization process is employed for the fabrication of AAO using Oxalic and Sulfuric electrolytes. The resulting porous network consists of nanopores with 40 and 80 nm diameters respectively. The AAO is used as a mask to nanopattern large areas (cm<sup>2</sup>) of solid substrates following a two-polymer transfer process. Initially, a sulfuric AAO was used for template assisted electrodeposition to assemble the first layer of Ni nanorods with an overgrown thin film. Subsequently, an oxalic AAO was transferred upon the Ni film. The electrodeposition was repeated using the Ni film as the working electrode to assemble the second vertical layer as seen in Figure 1A. Additionally, the nanorod's elemental composition was controlled by varying the electroplating solution (Ni, Co, Au). Repeating the same transfer procedure, segmented nanorods of Ni-Au and Co-Au were assembled into vertical layers as seen in Figure 1B. Cross sectional cuts were prepared using a milling procedure in a Zeiss Crossbeam 340 Focused Ion Beam combined with Scanning Electron Microscopy. The elemental composition of the segmented nanorods was evaluated using energy dispersive spectroscopy. Additionally, magnetic analysis of the ferromagnetic segments was performed using off axis electron holography. In this way, nanostructures with high complexity can be tailored to have desired aspect

ratios and varying chemical compositions for distinct functionalities and applications.

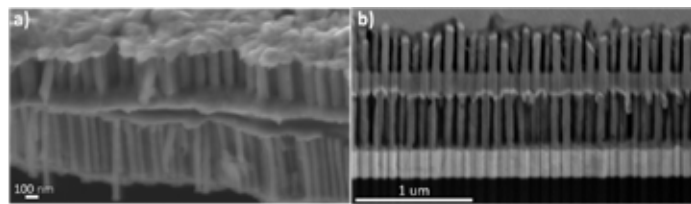


**Figure 1.** SEM images of bi-layer vertical stacking. A) We show total control of diameter with 40 and 80 nm Ni nanorods fabricated on bottom and top layers respectively. B) Control of chemical composition by assembling segmented Ni-Au and Co-Au nanorods on bottom and top layers respectively.

**NANOPARTICLE THERAPY AS A MEANS OF VECTOR-BORNE DISEASE CONTROL.** THELMA AMEH<sup>1</sup>, KUZY ZARZOSA<sup>1,2</sup>, TYLER VARZEAS<sup>1</sup>, BAILEY SHARP<sup>1</sup>, MATTHEW GIBB<sup>3</sup>, EVAN BRASWELL<sup>2</sup> and CHRISTIE SAYES<sup>1,3</sup>

<sup>1</sup>Department of Environmental Science, Baylor University, Waco, TX 76798; <sup>2</sup>Mission Laboratory, USDA APHIS PPQ CPHST, Edinburg, TX 78539; <sup>3</sup>Institute of Biomedical Studies, Baylor University, Waco, TX 76798

The spread of vector-borne pathogens by arthropod hosts continues to cause human, animal and plant diseases of public health and economic importance. Using the integrated vector management approach, this study utilizes nanoparticles as potential targeted anti-pathogenic agents for the control of citrus greening disease. *Candidatus liberibacter asiaticus*, the bacterial pathogen of citrus greening disease is spread by the Asian citrus psyllid (*Diaphorina citri Kuwayama*). Symptoms of the disease include blotchy mottle, yellow shoots, and improperly developed fruits. The significant decrease in edible fruit production caused by the disease has led to lower productivity of citrus farms, which, in turn, causes significant economic loss to the citrus industry. Silver nanoparticles were synthesized, and surface functionalized with charged and uncharged groups. The resulting nanoparticles had their size and shape measured, using dynamic light scattering (DLS), transmission electron microscopy (TEM), and atomic force microscopy (AFM). Ultraviolet-visible spectroscopy (UV-Vis) of nanoparticles was done to characterize the differences in surface coating of the nanoparticles followed by Fourier-transform infrared (FTIR) analyses for functional group characterization. Exposure studies carried out on the psyllid vector show differential accumulation of silver nanoparticles based on surface coating. Inductively coupled plasma mass spectrometry (ICPMS) shows that negatively charged silver nanoparticles coated with citrate had the highest accumulated concentration (8.27 μg/L) after 96 h of exposure through an artificial feeding media, compared to positively charged and uncharged silver nanoparticles. The results obtained from this study suggest that other

arthropods would have similar responses to nanoparticle exposure and that this approach of disease control may be translatable to other vectors of pathogenic diseases.

## EDUCATION/LIFE SCIENCES ABSTRACT Spring 2020

### SOME HARMFUL AND BENEFICIAL FUNGI: A MICROSCOPIC INVESTIGATION. LYANNA DELEON, CAITLIN RIVAS, AUBREY HOWARD AND NABARUN GHOSH.

Department of Life, Earth & Environmental Sciences,  
West Texas A&M University, Canyon, Texas 79015

Fungi have the ability to grow indoor and outdoor and can enter the house through open doorways, windows, vents, as well as heating and air conditioning systems. Concentration and composition of the airborne fungal spores are important in the diagnosis of Allergy and asthma cases in an area. We have used two different techniques to capture and collect the fungal samples. We used a Burkard Volumetric Spore Trap to capture the aeroallergen. It was placed on the third-floor roof of the Natural Science Building of the West Texas A&M University. We collected the spores on the Sellotape placed on the drum and stained them with 2% safranin and mounted the slide in Gelvatol. We observed the prepared slides using a BX-40 Olympus Microscope equipped with a DP-74 digital camera and the *Cellsens* software. We observed the frequent presence of conidia *Alternaria alternata*, *Stachybotrys*, *Drechslera* and ascospores. We also observed plenty of burnt residues, gums and resinous exudates from the plants and various forms of fibers. All these are considered as potential allergens and causal factors for allergic rhinitis and related symptoms. In the second part, we have collected the spoiled food materials and cheese. We stained the isolated fungal materials after a brief

flaming on an alcohol lamp. After staining with Lacto-phenol Cotton Blue stain, we observed the spores and mycelia produced by the fungi using a Leica DM-750 digital microscope equipped with LAS V4.9 software for capturing images. Micrographs were captured, analyzed and labeled accordingly. We observed *Rhizopus stolonifer*, *Colletotrichum truncatum*, *Aspergillus niger*, *Penicillium notatum* and various types of spores from Deuteromycetous fungi. Although various species of *Penicillium* cause lots of food spoilage, the first antibiotic Penicillin was discovered by Alexander Fleming and saved the lives of billions till to the date. Our continued research will include collection of fungal samples from different households, capturing images after staining suitably and analyzing them based on their spore morphology using the standard identification keys. This research will provide important data on the fungi that are prevalent in the households, causing illness to the dwellers and food spoilage. *Aspergillus tubingensis*, an apparently harmful food spoiling fungus may be an answer and solution to the present-day problem of plastic pollution.

### THE USE OF DIGITAL MICROSCOPY AND VOCATIONAL TRAINING IN SPECIAL EDUCATION TO IMPROVE THE QUALITY OF TEACHING. MARIA LOUISA ZAVALA<sup>1</sup>, SANDAR MAE GODWIN<sup>1,2</sup> and NABARUN GHOSH<sup>1</sup>

<sup>1</sup>Department of Life, Earth & Environmental Sciences,  
West Texas A&M University, Canyon, Texas 79015,

<sup>2</sup>Pampa ISD, Pampa, Texas 79065

This report covers two projects aimed to improve classroom teaching, with more hands-on and vocational experience, at public schools. The first one undertaken was the use of Digital Microscopy in teaching the Mitotic cell division. Currently, in most of the Biology classes, prepared slides are used to demonstrate the process of Mitosis in the onion root tips (1). We have chosen a hands-on activity to demonstrate this process in live onion root tips. It involved a 5-step technique,

### CALL FOR PAPERS

Authors are invited to submit their manuscripts for the next edition of the Texas Journal of Microscopy. The objective of the journal is to publish papers on original research and development of methods for providing prospect guidelines to research supported by all forms of microscopy. Please send your work as short communications, full articles or review articles in biological sciences, material sciences or education to either journal editor:

Catalina Pislariu  
[cpislariu@twu.edu](mailto:cpislariu@twu.edu)

Nabarun Ghosh  
[nghosh@wtamu.edu](mailto:nghosh@wtamu.edu)

in which the specimen is cut, washed, preserved, and stained in order to prepare the slides for observation and capture of digital micrographs to examine the different phases of Mitotic cell division. We excised the root tips from the control set of bulbs and pre-treated them with saturated solution of para-Dichlorobenzene (p-DB) for 3 hours. After pre-treatment, the root tips were washed with distilled water and fixed with 1:3 Acetone-ethanol overnight. The fixed root tips were stained with 2% Aceto-Orcein solution and squashed in 45% acetic acid<sup>1</sup>. Once the slide was prepared, we observed the different phases of cell division, and captured the micrographs at various magnifications using a BX-40 Olympus microscope equipped with CellSens software. We observed the best chromosome morphology revealed at the metaphase plate that was used for the karyotyping. While using the digital microscopy system, we opened the image with MS Photo Editor. We, then, clicked on the picture that we wanted to edit. Next, we focused and cropped the image to an area that we wanted to enhance. The captured image was modified to improve its visual quality. We labeled the image with the Paint 3D software. We used the 2D shapes button by clicking on the line adjustment to adjust the line thickness and size as necessary. When labeling, we selected text, created a text box and typed the necessary text and adjusted the size of the text box, and checked the spelling. We labeled the picture parts in the same way and saved the image for digital printing. The advantages of this type of experimental design is not only useful for the educators but for the students as well. In a classroom, students often do not get to see the real biological images of the cell division from living materials since the teaching tools in the classroom often consist of posters with cartoon images. This can put a person at a disadvantage in the workforce, as they are unable to identify what actual cell division looks like. Digital microscopy allows educators to project micrographs to the classroom all at once using projection techniques equipped with a microscope. This technology also demonstrates the recent advancement of the digital media as an asset and new way of educating the future students. With the flood of media and technologies, it is hard to keep students interested. However, incorporating new devices that are often a distraction in the classroom now become an asset to Education.

Technology is not the only way to educate students and prepare them for their life in the future. A vocational program was designed at the Pampa ISD, Texas to help the special education students to improve their everyday work skills (2). This continuous vocational training program is presently running at different worksites in the Texas Panhandle. We provide a contract that protects the employers and the school district signed by all three parties (parents, teachers, and employers). The students attending the program are high school graduates who

willingly sign up for the extended school program that they can attend until they are twenty-two. The goal and the mission of the 18+ vocational program is to assist students with acquiring various skills, which are necessary to transition into the real world. This includes job coaching at local approved vocational training sites. While at the approved job site, we have an employee show the students how to perform a specific job they receive training for. Students also have the opportunity to obtain daily living skills such as balancing a checking account, maintaining a budget, and obtaining a driver's license. Students practice mock interview skills, learn how to create qualified resumes, and use current vocational training as a form of work listed on their resumes. Students learn the skill of hotel management by working front desk computers, answering hotel phones, learning social skills by using appropriate manners when speaking to the hotel guests, and, in addition to that, they receive training with the housekeepers in that hotel. Students can also receive vocational training at a local car dealership. Skills that they obtain at the dealership include greeting customers with a smile, cleaning the cars and the parking lots, sweeping the floors, cleaning the windows, and filing and organizing the documents and papers. Our students also receive vocational training at Walmart. They stock shelves with merchandise, sweep floors, learn how to speak properly to the customers, and shadow employees. They can also receive training at a local convenience store, which allows them to unload trucks with store's merchandise, straighten shelves, and restock the refrigerators. Students that are not employable due to some constraints, obtain skills to help around their household such as folding laundry, doing dishes, and vacuuming and sweeping. Students also work on improving math, handwriting, and social skills that will be beneficial with their future employment. Students also list things they want to improve individually for guidance and correction. Our hope is to provide the support and education the students need while attending this program, but also to give the tools they need in order to be successful after finishing the program.

#### References:

1. Sharma, A.K., and Sharma, A. (1980) "Chromosome Technique: Theory and Practice," 3rd Ed., Butterworths, London, pp. 68-470.
2. Hennessey, M and Godwin S. (2019) The Pampa High School 18+ Program. Explore, Vol. 2, pp. 54-67.

## TECHNICAL ABSTRACTS Spring 2019

### COMPARISON OF CALCULATED AND MEASURED POINT SPREAD FUNCTIONS TOWARD ACCURATE SPACE-VARIANT MULTIVIEW DECONVOLUTION OF LARGE LIGHT-SHEET FLUORESCENCE MICROSCOPY DATA SETS. HOLLY C GIBBS, ALEX VERINO, DYLAN MCCREEDY, and KRISTEN MAITLAND

Microscopy and Imaging Center, Division of Research, Texas A&M University

Conventional light sheet fluorescence microscopy (LSFM) provides rapid, volumetric fluorescence imaging with cellular resolution. Common applications of LSFM are tracking morphogenic cellular movements of smaller, moderately transparent developing organisms (e.g. *Drosophila melanogaster*, zebrafish) and whole-organ imaging of larger clarified tissues (e.g. mouse spinal cord). To illuminate and observe a large field of view, LSFM optics are typically designed with low numerical aperture, yielding comparably poorer resolution than confocal microscopy. Deconvolution can provide a means to improve the resolution of these data sets for characterizing sub-cellular morphological details in such tissues. However, it may be problematic to apply the typical space-invariant approach to point spread functions (PSFs) generation or estimation under certain conditions. We propose to characterize variability of measured light sheet PSFs in aqueous environments of different refractive index (with and without perfectly index-matched optics) and compare these to computed light sheet PSFs. We further investigate the consequence of misapplying a spatially invariant PSF to deconvolve large data sets. These efforts may motivate the generation of deconvolution algorithms that apply a spatially-variant PSF to deblur light sheet fluorescence datasets and improve the accuracy of subsequent analysis of sub-cellular features.

### Micro-XRF FOR SEM... A COMPLEMENTARY APPROACH FOR EDS ANALYSIS IN THE SEM. STEPHAN BOEHM AND JOHN MASTOVICH BRUKER NANO INC., BILLERICA, MA

Micro- X-ray fluorescence spectroscopy [XRF] is a long known and complementary analytical technique to e-beam Energy Dispersive Spectroscopy [EDS] for the characterization of the elemental composition within unknown samples. With the introduction of the Bruker XTrace X-ray source, this technique becomes available for the Scanning Electron Microscope [SEM] user. Like the e-beam excitation, micro-XRF X-ray excitation analysis is a supplemental technique, which also delivers small area trace analysis information. The advantages of X-ray excitation are mainly the higher sensitivity for the detection of trace

elements, higher X-ray line excitation as well as information from greater depth within the sample. The availability of modern X-ray polycapillary optics enables the capability to focus X-rays to a spot size of less than 30  $\mu\text{m}$ , and contained in an X-ray source that can be mounted on an available SEM port, which uses the existing Bruker EDS detector (Figure 1). The SEM system then has dual beam potential i.e. both an e-beam and an X-ray beam, which offers new possibilities for the material characterization.



**Figure 1.** Example of XTrace setup on the SEM.

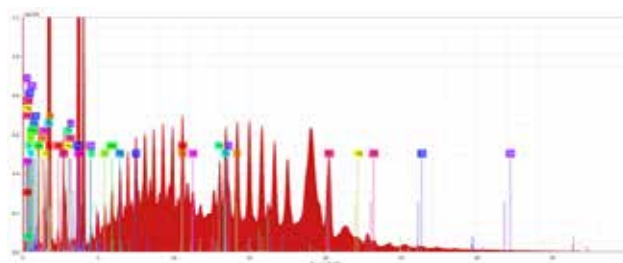


**Figure 2.** Spectrum of NIST 610 certified glass standard measured with XTrace on an SEM, illustrating the improved elemental P/B ratio by using X-ray excitation.

The SEM user can operate a micro-XRF system using similar parameters as an e-beam system, yielding results comparable with traditional SEM-EDS analysis, whilst obtaining additional information from the X-Ray-beam sample interaction. Electron excitation has a higher excitation efficiency for light elements, and it is possible to perform measurements down to Boron. X-ray excitation efficiency is better for heavy elements and allows the detection of traces even down to 10 ppm (Figure 2). The larger depth of X-ray excitation allows a deeper look inside the material, allowing the characterization of relatively thick layers or even of multilayer systems, ranging from 1nm to 40  $\mu\text{m}$ , which is not possible with electron excitation. Micro-XRF works with a fixed X-ray beam, consequently X-ray elemental distribution maps must be acquired via stage movement. Developments of adding a piezo-based stage mounted on top of the SEM stage enables high-speed elemental X-ray mapping over large areas (Figure 3). Seamlessly integrated into the Bruker ESPRIT software suite, XTrace even allows for simultaneous e-beam / micro-

XRF acquisition, incorporating light element spectral data as well as trace element and/or higher energy X-ray data (Figure 4).

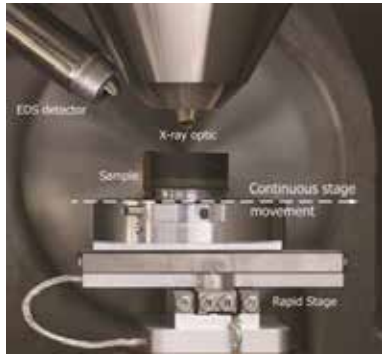


**Figure 3.** Example for X-ray Mapping setup in the SEM showing the Rapid Stage setup as well as the X-ray optic and EDS detector placement

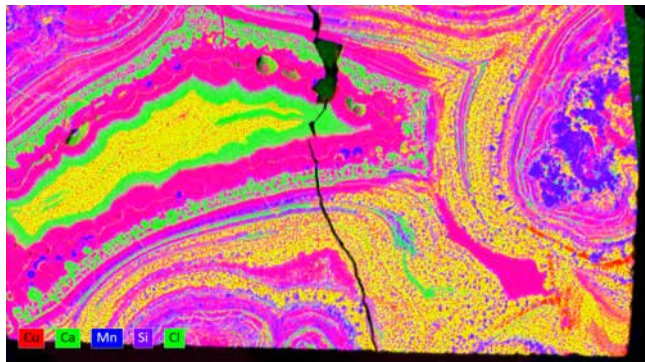


**Figure 4.** Large area X-ray map (45 mm x 30 mm) of an Exotic copper deposit sample aquired with XTrace, showing the element distribution information for Copper – Red, Calcium – Green, Manganese – Navy, Silicon – Purple, Chlorine – Dark green.

**ADVANCED STRUCTURAL CHARACTERIZATIONS AND STRAIN MEASUREMENTS IN MATERIALS AND MICROELECTRONIC DEVICES USING EBSD TECHNIQUE: THE INFLUENCE OF SAMPLE PREPARATION.** PAWEL NOWAKOWSKI, MARY RAY, PAUL FISCHIONE

E.A. Fischione Instruments, Inc., Export, PA, USA

Knowledge about strain, as well as its distribution in crystalline materials, is critical when studying phenomena such as stress fatigue, corrosion cracking, and formability. In semiconductor devices, elastic and plastic strain can introduce crystallographic defects and cause fracture and delamination, which can dramatically change electrical properties and device reliability. For these reasons, the measurement of plastic and elastic strain was widespread in industrial and academic environments in the past decade. Many techniques have been developed and used for plastic and elastic strain study (1-3). In microscopy and microanalyses, one of the techniques used for deformation structures characterization is electron backscatter diffraction (EBSD). EBSD plastic strain measurement

techniques rely on recording changes in EBSD pattern quality (4, 5) or local changes of crystal orientation within a grain (6, 7). The EBSD technique has recently been applied to elastic strain measurements. This approach is based on cross-correlation analysis of high- resolution EBSD patterns. The technique measures lattice distortion-related differences between reference EBSD pattern and pattern of interest, obtained from the same grain and it is known as HR-EBSD (8-10). Strain studies by EBSD and HR-EBSD are both very sensitive to diffraction pattern quality (11). Aside from intrinsic instrumentation limitations, sample preparation factors prominently into accuracy and precision attained in strain analyses (12-15). Surface contamination, oxidation, crystal lattice damage, and plastic deformation must be avoided during sample preparation to obtain accurate and precise measurements. A sample preparation technique that preserves the native state of the material microstructure, without introducing artifacts, is necessary to fully understand the failure mechanism.

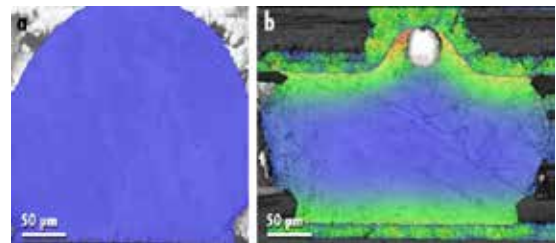


**Figure 1.** Strain contouring EBSD map of a solder joint after argon broad ion beam milling. Non-loaded solder joint (A) and loaded solder joint (B), which shows strain accumulated at the interface of the solder bump and copper pad and at the area between the solder bump void and copper pad.

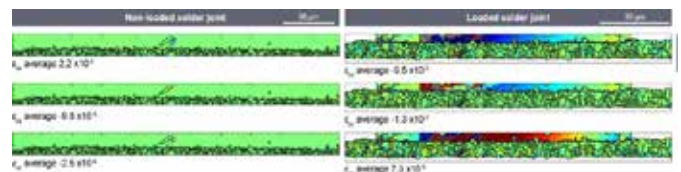


**Figure 2.** HR-EBSD strain field obtained for principal strain components:  $\epsilon_{xx}$ ,  $\epsilon_{yy}$ , and  $\epsilon_{zz}$  in a non-loaded solder joint (left) and a loaded solder joint (right).

In the presentation, we focus on the sample preparation of:

1. A bulk crystalline material (a nickel super alloy), with a focus on elastic strain associated with the  $\gamma/\gamma'$  interfaces.
2. A solder joint located between the package and the circuit board of a semiconductor device.

Two different sample techniques are described and compared: conventional mechanical polishing (MP) using colloidal silica suspension and broad ion beam (BIB) argon ion milling. Sample preparation is then confirmed by advanced structural characterizations and strain measurements, which are also explained in detailed.

Figure 1 compares strain in non-loaded and loaded

solder joints. Strain evaluated by local misorientation measurements shows an absence of deformation in the non-loaded sample (Figure 1A) and the presence of accumulated strain at the interface of the solder bump and copper pad in the loaded sample (Figure 1B). Figure 2 shows strain fields obtained for principal strain components:  $\epsilon_{xx}$ ,  $\epsilon_{yy}$ ,  $\epsilon_{zz}$  in a non-loaded solder joint (Figure 2A) and a loaded solder joint (Figure 2B). The presence of strain is associated with cracks and delamination at the solder joint interface, which provides insight into the failure mechanism.

## References

1. Wilkinson, A.J., and Dingley, D.J. (1991) Quantitative Deformation Studies Using Electron Back Scatter Patterns. *Acta Metallurgica Et Materialia* 39 (12): 3047-3055.
2. Kaboli, S., Demers, H., Brodusch, N. and Gauvin, R. (2013) Microstructural Characterization of Mg-Al-Ca Alloys Using Ion Milling Surface Preparation Technique. *Microscopy and Microanalysis* 19 (S2): 1756-1757.
3. Vaudin, M.D., Stan, G., Gerbig, Y.B. and Cook, Y.B. (2011) High Resolution Surface Morphology Measurements Using EBSD Cross-Correlation Techniques And AFM. *Ultramicroscopy* 111 (8): 1206-1213.
4. Wilkinson, A. J., Gonzalez, G. and Dingley, D.J. (1993) The Measurement of Local Plastic Deformation in a Metal-Matrix Composite by Electron Back-Scatter Patterns. *Journal of Microscopy* 169 (2): 255-261.
5. Masayuki, K., Wilkinson, A.J. and Titchmarsh, J.M. (2005) Measurement of Plastic Strain of Polycrystalline Material by Electron Backscatter Diffraction. *Nuclear Engineering and Design* 235 (6): 713-725.
6. Lehockey, E.M., Lin, Y-P., and Lepik, O.E. (2000) Mapping residual plastic strain in materials using electron backscatter diffraction, in *Electron backscatter diffraction in materials science*, edited by Adam J. Schwartz, Mukul Kumar, and Brent L. Adams, 2nd ed., 247-264. Boston: Springer.
7. Ørsund, R., Hjelen, J. and Nes, E. (1989) Local Lattice Curvature and Deformation Heterogeneities in Heavily Deformed Aluminium” *Scripta Metallurgica* 23 (7): 1193-1197.
8. Troost, K. Z., van der Sluis, P. and Gravesteijn D. J. (1993) “Microscale Elastic-Strain Determination by Backscatter Kikuchi Diffraction in The Scanning Electron Microscope”. *Applied Physics Letters* 62 (10): 1110-1112.
9. Wilkinson, A.J. (1996) Measurement of Elastic Strains and Small Lattice Rotations Using Electron Back Scatter Diffraction. *Ultramicroscopy* 62 (4): 237-247.
10. Wilkinson, A. J., Meaden, G. and Dingley, D.J. (2006) High-Resolution Elastic Strain Measurement from Electron Backscatter Diffraction Patterns: New Levels of Sensitivity. *Ultramicroscopy* 106 (4-5): 307-313.
11. Britton, T.B., and Wilkinson. A.J. (2011) Measurement of Residual Elastic Strain and Lattice Rotations with High Resolution Electron Backscatter Diffraction. *Ultramicroscopy* 111 (8): 1395-1404.
12. Nowakowski, P., Schlenker, J., Ray, M. and Fischione, P. (2016) Sample Preparation Using Broad Argon Ion Beam Milling for Electron Backscatter Diffraction (EBSD) Analysis. *Microscopy and Microanalysis* 22 (S3): 12-13.
13. Nowakowski, P., Bonifacio, C., Ray, M. and Fischione, P. (2019) Combining Emerging Sample Preparation Methods, SEM, And TEM Investigations for Microelectronics Device Characterization at Multiple Scales. *Microscopy and Microanalysis* 25 (S2): 688-689.
14. Nowakowski, P., Ray, M. and Fischione, P. (2019) Solder Bump Joint Failure Investigation: From Sample Preparation to Advanced Structural Characterizations and Strain Measurements. In *ISTFA 2019: Conference Proceedings from the 45Th International Symposium for Testing and Failure Analysis*, 43-47. Materials Park, OH: ASM International.
15. Nowakowski, P., Wizek, J., Bathula, V., Mielo, S., Khanal, S., Bonifacio, C. and Fischione, P. (2018) SEM And TEM Characterization of Plastic Deformation Structures in Aluminum By EBSD, TKD, And PED-Based Orientation Imaging Techniques”. *Microscopy and Microanalysis* 24 (S1): 2182-2183.



## SHORT COMMUNICATION

Spring 2020

### SURFACE TEXTURE ANALYSIS OF MELON RIND USING 3D RECONSTRUCTION FROM SEM STEREO IMAGES

STANISLAV VITHA<sup>1</sup>, SADHANA RAVISHANKAR<sup>2</sup>

<sup>1</sup> Microscopy and Imaging Center, Texas A&M University, College Station, TX 77843; <sup>2</sup> Department of Nutritional Sciences, University of Arizona, Tucson, AZ 85721

Melons are nutritious fruits with numerous health-promoting properties, offering important benefits for healthy diets. The major commercial melon varieties include the smooth-skinned honeydews (*Cucumis melo* L. *inodorus*) and cantaloupes (*C. melo* L. *reticulatus*), which exhibit a network of rougher, suberized tissue, referred to as the “net”. Episodes of foodborne illnesses from contamination with *Salmonella* and *Listeria*, associated mostly with netted melons, have hampered wider consumer acceptance. The physical characteristics of the surface of fruit, such as roughness and hydrophobicity, plays a role in bacterial attachment and resistance of bacteria to the cleaning and sanitization procedures (1,2). Therefore, analysis of fruit surface texture and the correlation with bacterial attachment is of much interest to growers, distributors and retailers. For this preliminary study, surface roughness of cantaloupe and honeydew melons was assessed using stereo images acquired via scanning electron microscopy. Digital elevation models (DEMs) constructed from the stereo images were used for profile and surface texture analysis in the Alicona MeX (Bruker Alicona, Austria) software.

Rind samples were excised, dehydrated in methanol and hexamethyldisilazane (HMDS) (3) and sputter coated

with 20 nm Au. Stereo images with 5% tilt were acquired with a Secondary Electron detector at 15 kV accelerating voltage and magnifications from 40x to 400x on a Tescan Vega 3 SEM (Tescan, Czech Republic) equipped with a compucentric stage. Images were imported into MeX software ver. 6.2.1. using the Stereo Creator module. The initial DEM was processed to remove form (plane tilt or surface curvature), and line and surface analysis was performed using a cut-off filter value of 500  $\mu\text{m}$  and 100  $\mu\text{m}$  for low and high magnification data, respectively.

The cantaloupe showed 2-fold higher roughness (Sq, root mean square deviation) than the honeydew, in low-magnification images that encompass both the netting and the epidermal patches between the netting (Figure 1). In higher magnification datasets, the smooth areas of cantaloupe rind were comparable in roughness to the honeydew sample. The netting on the cantaloupe surface showed roughness about three-fold higher than the smooth areas between the netting. This was the case in both line profilometry and in surface area analysis. These results suggested that the overall roughness of the cantaloupe surface is a product of the area occupied by netting.

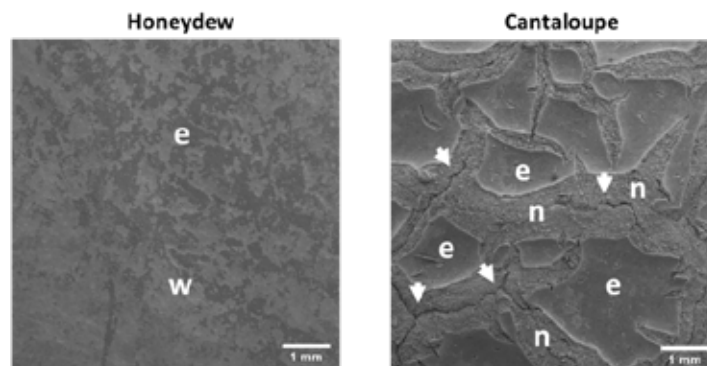


**Figure 1.** Honeydew and cantaloupe surface features. e: epidermis (smooth surface); w: crystalline waxy cuticle; n: netting (rough surface); arrows: deep fissures in the netting

#### References

1. Fernandes, P.E., Jose, J.F.B.S., Zerdas, E.R.M.A., Andrade, N.J., Fernandes, C.M., Silva, L.D. (2014) Influence of the hydrophobicity and surface roughness of mangoes and tomatoes on the adhesion of *Salmonella enterica* serovar *Typhimurium* and evaluation of cleaning procedures using surfactin. *Food Control*, 41:21-26.
2. Wang, H., Feng, H., Liang, W., Luo, Y., Malyarchuk, V. (2009) Effect of surface roughness on retention and removal of *Escherichia coli* O157:H7 on surfaces of selected fruits. *Journal of Food Science* 2009, 74:E8-E15.
3. Neinhuis, C., Edelmann, H.G. (1996) Methanol as a rapid fixative for the investigation of plant surfaces by SEM. *J. Microsc.*, 184:14-16.

# SCANNING ELECTRON AND CONFOCAL LASER SCANNING MICROSCOPY OF IN VITRO PREPARATIONS OF HAIR CELLS FROM THE MOUSE COCHLEAR SPIRAL

YANG YANG<sup>1</sup>, PRESTON L. SIMPSON<sup>1</sup>, LESLIE CLIMER<sup>1</sup>, BERND ZECHMANN<sup>3</sup>, DWAYNE D. SIMMONS<sup>1,2</sup>

<sup>1</sup>Departments of Biology, Baylor University, Waco, TX

<sup>2</sup>Psychology/Neuroscience, Baylor University, Waco, TX

<sup>3</sup> Center for Microscopy and Imaging (CMI), Baylor University, Waco, TX

In the mammalian cochlea, auditory hair cells act as sensory receptors and are located within the organ of Corti on a thin basilar membrane. In the organ of Corti, hair cells are divided into 3 rows of outer hair cells (OHCs) and 1 row of inner hair cells (IHCs). OHCs amplify low-level sounds by using active movements of their cell bodies and stereocilia (hair bundles), while IHCs transform vibration caused by sound waves into neural signals. OHC amplification is modulated by intracellular calcium signals. Oncomodulin (OCM,  $\beta$ -parvalbumin), an EF-hand calcium binding protein (CaBP), is expressed predominantly by OHCs and alters OHC calcium signals. OCM shares 53% sequence homology with  $\alpha$ -parvalbumin ( $\alpha$ PV), which is also expressed in immature and young adult OHCs. In mice,  $\alpha$ PV expression occurs as early as embryonic day

18, whereas OCM expression occurs postnatally. OCM is the only known CaBP for which targeted deletion (OCM knockout [KO]) causes progressive hearing loss. We observed hair bundles from OHCs of postnatal mice using scanning electron microscopy (SEM) (Figure 1A & B). Using confocal laser scanning microscopy (CLSM), OHCs from wild type (WT) and OCM KO mice with a targeted knock-in of a Ca<sup>2+</sup> sensor (GCaMP6s) were analyzed (Figure 1C). There are no apparent morphological differences between hair cells in postnatal OCM WT and KO mice. However, the absence of OCM in OHCs alters both OHC calcium signaling and the relative expression of purinergic receptors, which are calcium transporters. These results are consistent with OCM playing a significant role in OHC function.

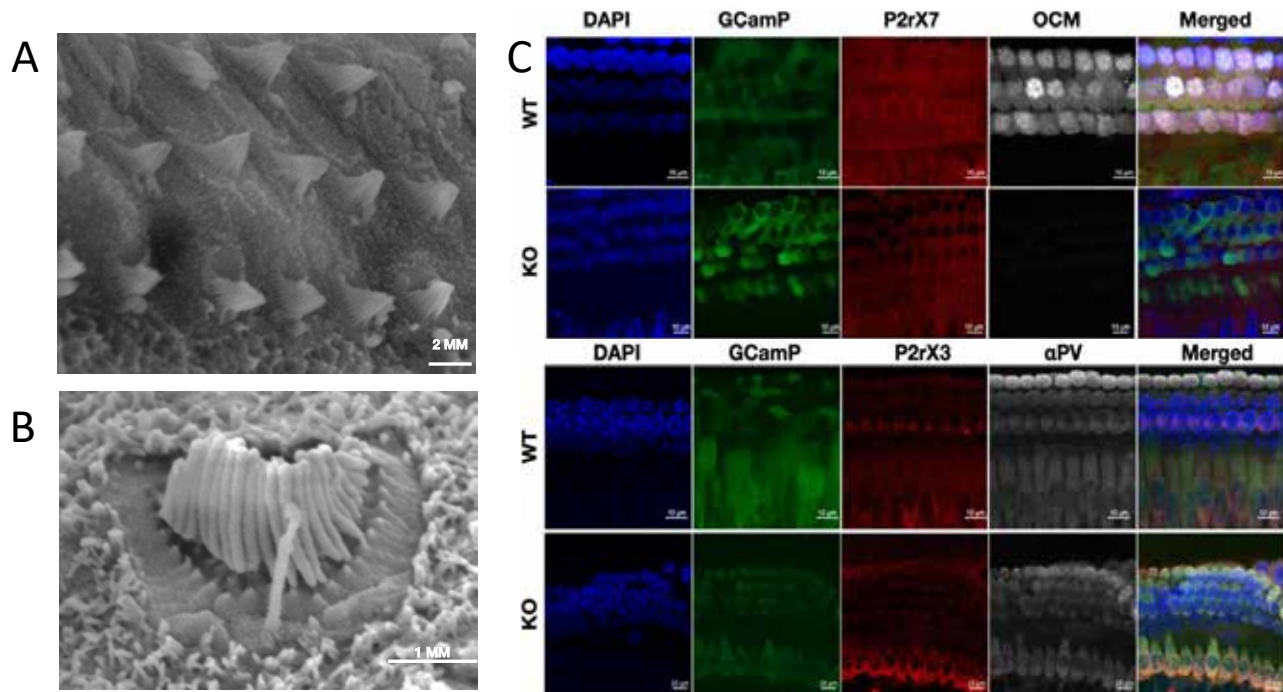


**Figure 1.** Outer hair cells (OHCs) morphology in wild-type and OCM knockout GCaMP6s mice. Panels A shows hair bundles from the isolated organ of Corti. A single hair bundle with highly ordered stereocilia and kinocilium is shown in B. Photomicrographs in panels A and B were acquired using an SEM. C) Maximum intensity projections (MIPs) generated from high-resolution images of OHCs (~7  $\mu$ m) were acquired from GCaMP6s-positive mice in the cochlear apex. Single channel and merged images were acquired by CLSM.

A FLUORESCENCE-BASED REPORTER OF ARGINYLTRANSFERASE 1 (ATE1)

YASAR ARFAT T KASU, RINKI DASGUPTA, AND CHRISTOPHER S BROWER

Department of Biology , Texas Woman's University, Denton, Texas

**Abstract**

Arginyltransferase 1 (ATE1) is an enzyme that catalyzes the transfer of arginine onto protein fragments with acidic N-termini. This is an essential step in the degradation of these fragments by the N-degron pathway of the ubiquitin proteasome system. Previous studies have shown that arginylation is required for the removal of specific fragments associated neurodegeneration, and that the loss of ATE1 activity leads to neurological problems. Interestingly, reduced ATE1 activity was also associated with fat loss and resistance to diet-induced obesity. Thus, the modulation of ATE1 holds promise for treating these increasingly common human diseases. To this end, we synthesized a cell-based reporter that employs direct fluorescence to monitor ATE1 activity. Using confocal microscopy and immunoblot analysis, we show that this reporter provides a robust readout of ATE1 activity *in vivo*. This reporter will be useful in screening approaches aimed to identify modulators of ATE1, which may ultimately have therapeutic potential.

**Keywords:** arginylation, ubiquitin proteasome system, N-degron pathway, fluorescence microscopy

**Introduction**

The temporal and spatial regulation of protein function often occurs by way of non-processive protein cleavage. This generates protein fragments that, if not removed, can lead to cellular toxicity due to aberrant functions or aggregation. The removal of damaged proteins is carried out largely by the ubiquitin-proteasome system (UPS) which marks proteins for degradation by the proteasome through the covalent attachment of ubiquitin (Ub) (1). A specific UPS pathway that degrades protein fragments is called the N-degron pathway (formerly called the N-end rule pathway). In this pathway, protein fragments bearing N-terminal basic (e.g. Arg, Lys, or His) or bulky hydrophobic amino acids (e.g. Phe, Lue, Trp, Tyr, or Ile) are recognized by the ubiquitin recognin box (UBR) family of Ub-ligases. These ligases facilitate the poly-ubiquitylation and proteasomal degradation of the fragments. N-terminal Asn, Gln, Asp, Glu, and Cys are also destabilizing, but they require enzymatic modifications. These modifications include deamidation of Asn and Gln by NTAN1 and NTAQ1, respectively, and N-terminal arginylation of Asp, Glu, and oxidized Cys, carried out solely by the *Ate1*-encoded arginyltransferase 1 (ATE1) (2-4).

There is mounting evidence demonstrating the role of arginylation in a number of physiological processes. It was found that deletion of the *Ate1* gene in mice resulted in embryonic lethality resulting from cardiovascular defects (5). Subsequent studies using conditional knockout mouse strains found that the loss of post-natal *Ate1* gene function resulted in a marked loss of fat and resistance to high-fat diet-induced obesity (4). There is also evidence that arginylation plays a role in nervous system development as well as in maintaining brain function and preventing neurodegeneration (4, 6). We found that the N-degron pathway can degrade specific fragments of aggregation-prone proteins associated with amyotrophic lateral sclerosis

(ALS), frontotemporal dementia (FTD), Alzheimer's disease, and Parkinson's disease (7). We also found that in the absence of ATE1, C-terminal fragments of the TAR DNA-binding protein-43 (TDP43) form intracellular aggregates similar to those identified in patients with ALS and FTD (8). Given these findings, we expect ATE1 to be an effective therapeutic target for both obesity and neurodegeneration.

There is great interest in discovering pharmacological modulators of the UPS. Indeed, inhibitors of the proteasome have shown success in treating multiple myeloma and breast cancer (9-12). As the proteasome is the final step in the UPS-mediated degradation of a large variety of proteins, inhibitors of specific upstream steps are expected to have fewer off-target effects and greater specificity. For example, inhibitors of ATE1 would stabilize only a subset of proteins degraded by the N-degron pathway and would leave the bulk of UPS-mediated degradation unperturbed. Several natural and synthetic inhibitors of UBR proteins and ATE1 have been described; however, they were either identified through *in vitro* screening systems and do not work well *in vivo*, or they have low specificity (13-22). For example, tannic acid, a naturally occurring plant-derived polyphenol found in tea and red wine, was shown to inhibit ATE1 activity (23). However, tannic acid causes a wide range of cellular effects and has a growing list of molecular targets (24). As such, there is a need for *in vivo* screening methods to identify compounds capable of penetrating cells and with regulatory function restricted to specific steps in protein degradation. To that end, we have developed a highly sensitive, cell-based, dual-fluorescent reporter that provides a "digital" signal of ATE1 activity *in vivo*. This reporter can be employed in the search for pharmacological or genetic modulators of ATE1 that may have therapeutic benefit in the treatment of human diseases such as obesity and neurodegeneration.

## Materials and methods

**Synthesis of a dual fluorescent reporter for ATE1.** To generate the URT-based plasmid pYK17 encoding mCherry-Ub-Ndeg-GFP, the Q5 site directed mutagenesis kit (New England Biolabs) was used according to the manufacturer's protocol to remove the cDNA encoding human TDP43 amino acids 264 to 414 from pYK08 encoding mCherry-Ub-TDP43<sup>247</sup>-eGFP. Briefly, pYK08 was amplified (25 cycles) using primers, 5-GGTTCAATGGTGAGCAAGGGC-3 (forward primer) and 5-CTTAGGTTCCGGCATTGGATATATG AACGC-3 (reverse primer), then 1 µl of the PCR product was incubated in Kinase-DpnI-Ligase (KDL) reaction for 10 min at room temperature to remove the pYK08 template and ligate pYK17. NEB5α cells (New England Biolabs) were transformed with the ligation mix and clones were selected on LB medium agar plates supplemented with 100 µg/ml ampicillin.

**Cell culture and transfection.** Wild type and CRISPR/Cas9-mediated *Ate1*-lacking (8) neuroblastoma cells (Neuro2a) cells were maintained at 37°C and 5% CO<sub>2</sub> in Dulbecco's Modified Eagle's Medium (Corning) containing 10% fetal bovine serum, 100U/ml penicillin, 0.1U/ml streptomycin and 20mM glutamine. At 80% confluency, cells were passaged and plated to poly-D-lysine coated plates for experiments. For transient transfection of pYK17, cells at ~75% confluency were transfected using BioT (Bioland Scientific) according to manufacturer's protocol. For proteasome inhibition, cells were treated with 10 µM MG132 (Cayman Chemical) for 6 hours before lysis.

**Lysate preparation and immunoblot analysis.** Cells were harvested and lysed in tissue lysis buffer (TLB) (50 mM HEPES, 10% glycerol, 0.05% NP-40, 150 mM NaCl, 1 mM DTT, and 1 mM phenylmethylsulfonyl fluoride containing the complete protease inhibitor mixture (Thermo Scientific)) by freezing-thawing. The lysate was then centrifuged at 13,000 rpm for 20 min at 4°C, and the supernatant was collected. Protein concentrations were determined by using the Bio-Rad protein assay reagent according to the manufacturer's protocol. For immunoblotting, sample protein concentrations were normalized, heated to 95°C for 5 min in 2x Laemmli buffer, separated on 4-to-12% gradient NuPage Bis-Tris premade gels (Invitrogen), and transferred onto a methanol-activated PVDF membrane (Bio-Rad) in Towbin buffer (25 mM Tris, 192 mM glycine, and 20% methanol). Membranes were blocked in 5% milk in phosphate buffered saline (PBS) containing 0.1% Tween 20 at room temperature for 1 h. Membranes were then incubated with an anti-GFP (1:4000 dilution; Abcam) or anti-GADPH (Santa Cruz Biotech) antibody for 4 hours, washed three times in PBS containing 0.1% Tween 20 for 5 min, and then incubated with secondary antibodies (1:7,000 dilution) for 1 h at room temperature. Thereafter, blots were washed three times with PBS containing 0.1% Tween 20 and twice in PBS and developed by using the Licor Odyssey CLx system.

**Immunocytochemistry.** Cells were fixed in 4% formaldehyde and washed three times with PBS and mounted in 4,6-diamidono-2-phenylindole (DAPI)-containing Vectashield mounting medium (Vector Laboratories). Fluorescent cells were imaged and quantified using a Nikon A1 confocal microscope and Nikon instrument software elements AR-3.2 imaging software.

## Results

To develop a fluorescent reporter highly sensitive to ATE1 activity, we generated an unstable green fluorescent protein (GFP) that is degraded in an ATE1-dependent manner. For this, we exploited TDP43<sup>247</sup>, a specific aggregation-prone fragment of human TDP43 (amino acids 247 - 414) that was shown to be deposited in the brains of patients with FTD (25). We previously reported that TDP43<sup>247</sup> was ubiquitylated and degradation by the N-degron pathway in an ATE1-dependent manner (7, 8). Initially, we fused GFP to the C-terminus of TDP43<sup>247</sup> to generate TDP43<sup>247</sup>-GFP (Figure 1A). Through immunoblot analysis using an anti-GFP antibody, TDP43<sup>247</sup>-GFP could not be detected in extracts from wild type Neuro2a cells unless they were treated with the proteasome inhibitor MG132 (Figure 1A). On the other hand, proteasome inhibition was not required to detect TDP43<sup>247</sup>-GFP in extracts from Neuro2a cells that had undergone CRISPR/Cas9-mediated *Ate1*-knockout (ATE1-KO). This result indicated that, similar to TDP43<sup>247</sup>, TDP43<sup>247</sup>-GFP was degraded by the N-degron pathway in a manner that required ATE1. Confocal fluorescence microscopy of TDP43<sup>247</sup>-GFP in ATE1-KO cells revealed that it readily forms aggregates, precluding its usefulness as a soluble reporter (Figure 1B).

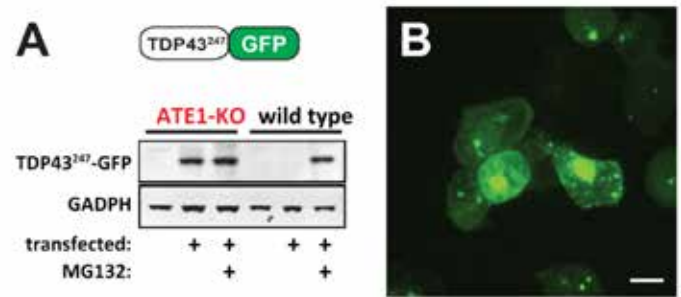


**Figure 1.** TDP43<sup>247</sup>-GFP is sensitive to ATE1 but aggregates in cells. **A)** Upper, schematic of TDP43<sup>247</sup>-GFP fusion protein. Lower, SDS-PAGE and immunoblotting using an anti-GFP antibody to detect steady-state levels of TDP43<sup>247</sup>-GFP expressed in wild type and ATE1-knockout (ATE1KO) Neuro2a cells treated in the presence or absence of the proteasome inhibitor, MG132. Note that TDP43<sup>247</sup>-GFP is detected in wild type cells only in the presence of MG132, whereas MG132 is not required for its detection in ATE1-KO cells. Lower panel shows anti-GADPH immunoblot.

**B)** Aggregation of TDP43<sup>247</sup>-GFP in ATE1-KO cells produces insoluble fluorescent aggregates. Bar, 10 µm.

In subsequent efforts, we replaced TDP43<sup>247</sup> with the minimal TDP43 sequence (amino acids 247-DLIKGISVHISNAEPK-263) needed for ATE1-dependent degradation. This sequence is referred to as the N-terminal degradation signal or "Ndeg" (Figure 2A). The ubiquitin reference technique (26) was used to express Ndeg-GFP bearing N-terminal Asp, the natural N-terminal amino acid of TDP43<sup>247</sup> that is arginylated by ATE1 (Figure 2A). For this, the cDNA encoding mCherry-Ub was cloned upstream and in-frame with Ndeg-GFP. The URT-based fusion was expressed as a single transcript, which was co-translationally cleaved by intracellular deubiquitylases (DUBs). This produces, at initially equimolar ratio, Ndeg-

GFP, which is unstable in the presence of ATE1, and the stable “reference” protein, mCherry-Ub, which marks transfected cells. Ratiometric fluorescence of GFP to mCherry allows for a quantitative measurement of ATE1 activity.

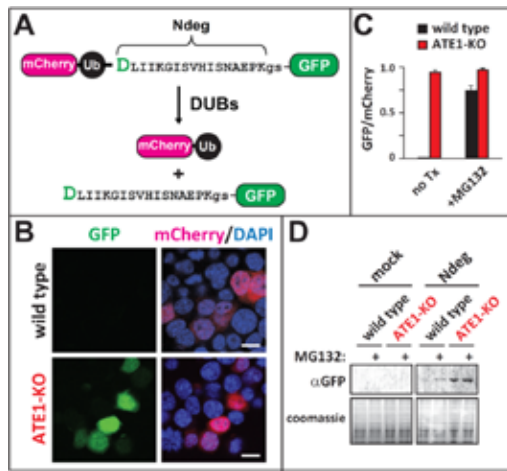


**Figure 2.** Ndeg-GFP is a soluble and robust reporter for ATE1 activity. **A**) mCherry-based URT expression of Ndeg-GFP. Co-translational cleavage of mCherry-Ub-Ndeg-GFP by intracellular deubiquitylases (DUBs) produces Ndeg-GFP, which is unstable in the presence of ATE, and mCherry-Ub, a stable internal reference, at initial equimolar ratio. Ratiometric fluorescence allows for the quantitative measurement of ATE1 activity. **B**) Ndeg-GFP is degraded in WT cells but detected as diffuse fluorescence in ATE1-KO cells. Bars, 10  $\mu$ m. **C**) The ratio of Ndeg-GFP-positive cells divided by mCherry-positive cells in the presence (+MG132) or absence (no Tx) of MG132. **D**) SDS-PAGE and immunoblotting using an anti-GFP antibody to detect steady-state levels of Ndeg-GFP expressed in wild type and ATE1-KO Neuro2a cells treated with a proteasome inhibitor MG132. Samples were in duplicates. The lower panels show coomassie staining of the membrane to indicate equal loading.

To determine the *in vivo* aggregation propensity and degradation of Ndeg-GFP, we examined its fluorescence in wild type and ATE1-KO Neuro2a cells using confocal microscopy. Similar to TDP43<sup>247</sup>-GFP, Ndeg-GFP was not detected in transfected wild type cells but were easily detected in transfected ATE1-KO cells (transfected cells were marked by mCherry) (Figure 2B). In contrast to TDP43<sup>247</sup>-GFP, Ndeg-GFP was detected as diffuse fluorescence (compare Figure 2B to Figure 1B). These results indicate that Ndeg-GFP is a soluble reporter for ATE1 activity.

In order to determine the sensitivity of the Ndeg-GFP reporter, we counted the number of mCherry-positive wild type and ATE1-KO Neuro2a cells in which green fluorescence was detected. Signifying its robustness, Ndeg-GFP was detected in 95.4% of mCherry-positive ATE1-KO but was undetected in mCherry-positive wild type cells (Figure 2C). When treated with the proteasome inhibitor MG132, Ndeg-GFP was detected in 100% of mCherry-positive ATE1-KO and in 75.5% of mCherry-positive wild type cells (Figure 2C). This result indicates that Ndeg-GFP is degraded by the UPS and ATE1 is required.

To examine Ndeg-GFP expression using another method, we separated cell extracts from transfected wild

type and ATE1-KO Neuro2a cells by SDS-PAGE and carried out immunoblot analysis using an anti-GFP antibody. Similar to TDP43<sup>247</sup>-GFP, Ndeg-GFP expression was only detected in extracts from wild type cells treated with the proteasome inhibitor, MG132 (Figure 2D). On the other hand, proteasome inhibition was not required for detection of Ndeg-GFP in extracts from ATE1-KO cells. Together, the above results demonstrate that fluorescence produced by Ndeg-GFP is inversely related to ATE1 activity; therefore, Ndeg-GFP functions as a robust reporter of ATE1 in cells.

## Discussion

To develop a fluorescent reporter capable of detecting ATE1 activity *in vivo*, we generated Ndeg-GFP, a variant of GFP that is unstable in the presence of ATE1. Ndeg is the minimal TDP43 sequence (amino acids 247 - 263) required for arginylation and degradation by the N-degron (8). Although substrate recognition by ATE1 and UBRs occur largely through the first two N-terminal residues (27, 28), Ndeg extends seventeen residues to Lys263, which is the preferred site of poly-Ub attachment (8). In order to express Ndeg-GFP, bearing N-terminal Asp (as opposed to N-terminal Met), and a separate fluorescent reporter with different excitation and emission spectra, we expressed it in a linear fusion with mCherry-Ub using the ubiquitin reference technique (Figure 2A) (26). Whereas the stability of Ndeg-GFP is determined by ATE1, mCherry-Ub is stable and can be used to mark cells transfected with the reporter. This design also enables ratiometric fluorescence, which reduces false positives by normalizing off-target effects such as those on transcription, translation, or cell fitness. We envision this reporter will be useful in unbiased screening applications using either pooled or arrayed platforms. For example, stable cell lines expressing Ndeg-GFP can be used in genetic screens (e.g. CRISPR/Cas9 knockout screens) or in fully automated, high-throughput compound library screens for modulators with *in vivo* efficacy. Activators of ATE1 are predicted to decrease the GFP/mCherry ratio, whereas inhibitors should increase the ratio. In addition, this reporter can be used in experiments to determine if ATE1 is regulated in a context-specific manner (e.g. cell cycle or stress).

The expression level of the reporter as well as the cell type used in specific screening applications should be tailored to the desired outcomes. For example, a screen for inhibitors of ATE1 should be carried out with Ndeg-GFP expressed from a relatively weak promoter (so as not to exhaust degradation machinery) and in cells that have robust N-degron activity. In this report, the URT-based mCherry-Ub-Ndeg-GFP construct was expressed using the mouse prion promoter as it generates adequate levels of mCherry-Ub and Ndeg-GFP for easy detection, but does not exhaust degradation machinery in Neuro2a cells. Clonally derived, stable cell lines using this reporter should be validated on an individual basis by comparing fluorescence ratios in the presence and absence of proteasomal inhibition to determine the sensitivity of the reporter cell line.

The design of this reporter also incorporates additional features that are beneficial in screening applications. Due to the hierarchical nature of the N-degron pathway (29), otherwise identical Ndeg-GFP reporters bearing alternative N-terminal amino acids can be used to target alternative

steps in the N-degron pathway or in orthogonal screens to validate modulators and help determine their “mode of action”. Here, we use Ndeg-GFP bearing N-terminal Asp (Asp-Ndeg-GFP) so that its degradation would depend on ATE1. Asn-Ndeg-GFP or Gln-Ndeg-GFP, on the other hand, can be used to identify modulators of NTAN1 or NTAQ1, respectively. Modulators that influence the stability of Leu-Ndeg-GFP, for example, will likely regulate the N-degron pathway downstream of ATE1.

Summing up, we have generated and validated a robust, cell-based, dual-fluorescent reporter to identify modulators of ATE1. Downstream applications of this reporter include its use in the search for inhibitors and activators of ATE1, which may ultimately have therapeutic potential to treat human diseases such as obesity and neurodegeneration.

## References

1. Varshavsky, A. (2012) The ubiquitin system, an immense realm. *Annual review of biochemistry*. 81:167-76.
2. Tasaki, T., Sriram, S.M., Park, K.S., Kwon, Y.T. (2012) The N-end rule pathway. *Annual review of biochemistry*. 81:261-89.
3. Varshavsky, A. (2011) The N-end rule pathway and regulation by proteolysis. *Protein Science*. 20:1298-345.
4. Brower, C.S., Varshavsky, A. (2009) Ablation of arginylation in the mouse N-end rule pathway: loss of fat, higher metabolic rate, damaged spermatogenesis, and neurological perturbations. *PLoS One*. 4(11):e7757.
5. Kwon, Y.T., Kashina, A.S., Davydov, I.V., Hu, R.G., An, J.Y., Seo, J.W., Du F., Varshavsky, A. (2002) An essential role of N-terminal arginylation in cardiovascular development. *Science*. 297(5578):96-9.
6. Wang, J., Pavlyk, I., Vedula, P., Sterling, S., Leu, N.A., Dong, D.W., Kashina, A.S. (2017) Arginyltransferase ATE1 is targeted to the neuronal growth cones and regulates neurite outgrowth during brain development. *Developmental Biology*. 430(1):41-51.
7. Brower, C.S., Piatkov, K.I., Varshavsky, A. (2013) Neurodegeneration-associated protein fragments as short-lived substrates of the N-end rule pathway. *Molecular Cell*. 50(2):161-71.
8. Kasu, Y.A.T., Alemu, S., Lamari, A., Loew, N., Brower, C.S. (2018) The N-termini of TAR DNA-binding protein-43 (TDP43) C-terminal fragments influence degradation, aggregation propensity and morphology. *Molecular Cell Biology*. 38(19):e00243-18.
9. Guang, M.H.Z., Kavanagh, E.L., Dunne, L.P., Dowling, P., Zhang, L., Lindsay, S., Bazou, D., Goh, C.Y., Hanley, C., Bianchi, G., Anderson, K.C., O’Gorman, P., McCann, A. (2019) Targeting Proteotoxic Stress in Cancer: A Review of the Role that Protein Quality Control Pathways Play in Oncogenesis. *Cancers*. 11(1). doi: 10.3390/cancers11010066.
10. Bastola, P., Oien, D.B., Cooley, M., Chien, J. (2018) Emerging Cancer Therapeutic Targets in Protein Homeostasis. *The AAPS Journal*. 20(6):94.
11. Brunnert, D., Kraus, M., Stuhmer, T., Kirner, S., Heiden, R., Goyal, P., Driessen, C., Bargou, R.C., Chatterjee, M. (2019) Novel cell line models to study mechanisms and overcoming strategies of proteasome inhibitor resistance in multiple myeloma. *Biochimica et Biophysica Acta Molecular Basis of Disease*. doi: 10.1016/j.bbadis.2019.04.003.
12. Park, J.E., Park, J., Jun, Y., Oh, Y., Ryoo, G., Jeong, Y.S., Gadalla, H.H., Min, J.S., Jo, J.H., Song, M.G., Kang, K.W., Bae, S.K., Yeo, Y., Lee, W. (2019) Expanding therapeutic utility of carfilzomib for breast cancer therapy by novel albumin-coated nanocrystal formulation. *Journal of Controlled Release* 302:148-59.
13. Kwon, Y.T., Levy, F., Varshavsky, A. (1999) Bivalent inhibitor of the N-end rule pathway. *Journal of Biological Chemistry*. 274(25):18135-9.
14. Lee, M.J., Pal, K., Tasaki, T., Roy, S., Jiang, S., An, J.Y., Banerjee, R., Kwon, Y.T. (2008) Synthetic heterovalent inhibitors targeting recognition E3 components of the N-end rule pathway. *Proceedings of the National Academy of Sciences USA*. 105:100-5.
15. Kitamura, K. (2015) Inhibition of the Arg/N-end rule pathway-mediated proteolysis by dipeptide-mimetic molecules. *Amino Acids*. 48(1):235-43.
16. Lee, J.H., Jiang, Y., Kwon, Y.T., Lee, M.J. (2015) Pharmacological Modulation of the N-End Rule Pathway and Its Therapeutic Implications. *Trends in Pharmacological Sciences*. 36(11):782-97.
17. Jiang, Y., Choi, W.H., Lee, J.H., Han, D.H., Kim, J.H., Chung, Y.S., Kim, S.H., Lee, M.J. (2014) A neurostimulant par-chloroamphetamine inhibits the arginylation branch of the N-end rule pathway. *Scientific Reports*. 4:6344.
18. Kopitz, J., Rist, B., Bohley, P. (1990) Post-translational arginylation of ornithine decarboxylase from rat hepatocytes. *The Biochemical Journal*. 267(2):343-8.
19. Kato, M. (1983) Heparin as an inhibitor of L-arginyl-tRNA: protein arginyltransferase. *Journal of Biochemistry*. 94(6):2015-22.
20. Yu, M., Chakraborty, G., Grabow, M., Ingoglia, N.A. (1994) Serine protease inhibitors block N-terminal arginylation of proteins by inhibiting the arginylation of tRNA in rat brains. *Neurochemical Research*. 19(1):105-10.
21. Li, J., Pickart, C.M. (1995) Inactivation of arginyl-tRNA protein transferase by a bifunctional arsenoxide: identification of residues proximal to the arsenoxide site. *Biochemistry*. 34(1):139-47.
22. Hu, R-G., Wang, H., Xia, Z., Varshavsky, A. (2008) The N-end rule pathway is a sensor of heme. *Proceedings of the National Academy of Sciences USA*. 105:76-81.
23. Saha, S., Wang, J., Buckley, B., Wang, Q., Lilly, B., Chernov, M., Kashina, A. (2012) Small molecule inhibitors of arginyltransferase regulate arginylation-dependent protein degradation, cell motility, and angiogenesis. *Biochemical Pharmacology*. 83(7):866-73.
24. Braidy, N., Jugder, B.E., Poljak, A., Jayasena, T., Nabavi, S.M., Sachdev, P., Grant, R. (2017) Molecular targets of Tannic Acid in Alzheimer’s disease. *Current Alzheimer Research*. doi: 10.2174/1567205014666170206163158.
25. Nonaka, T., Kametani, F., Arai, T., Akiyama, H., Hasegawa, M. (2009) Truncation and pathogenic mutations facilitate the formation of intracellular aggregates of TDP-43. *Human Molecular Genetics*. 18(18):3353-64.
26. Choi, W.S., Jeong, B.-C., Joo, Y.J., Lee, M-R., Kim, J., Eck, M.J., Song, H.K. (2010) Structural basis for the recognition of N-end rule substrates by the UBR box of ubiquitin ligases. *Nature Structural & Molecular Biology*. 17:1175-81.
27. Wadas, B., Piatkov, K.I., Brower, C.S., Varshavsky, A. (2016) Analyzing N-terminal arginylation through the use of peptide arrays and degradation assays. *The Journal of Biological Chemistry*. 291(40):20976-92.
28. Lévy, F., Johnsson, N., Rüménapf, T., Varshavsky, A. (1996) Using ubiquitin to follow the metabolic fate of a protein. *Proceedings of the National Academy of Sciences USA*. 93:4907-12.

# JOIN THE TEXAS SOCIETY FOR MICROSCOPY ON FACEBOOK



**Dear TSM-members,**

Attached you will find the final call for the 54th meeting of our society in San Antonio from February 21st through 23rd, 2019. The attachments include detailed information for online registration, abstract submission, invited speakers, hotel reservation, and the social reception at Palenque Grill. Additionally, you will find information about the workshops which will be organized at the Kleberg Advanced Microscopy Center at The University of Texas at San An... [See More](#)

**Final Call for Abstracts**

All members are encouraged to present their research or professional accomplishments at our meeting. This can be done in 10-minute or 20-minute oral sessions, including poster presentations. In addition, abstracts can be presented at poster sessions (abstract presentation - 2019). Full information on abstract preparation, online registration and abstract submission can be found on the TSM website.

[www.texasmicroscopy.org](http://www.texasmicroscopy.org)

**Registration Information**

Workshop and live track on Thursday

- Dinner Reception
- Student Session
- Posters Presentation
- Poster Session
- Graduate Student's Social Reception
- Friday & Saturday Breakfast
- Friday Luncheon & Dinner Meeting
- Friday Luncheon & Dinner Meeting

**Abstract Submission**

Abstract submission deadline: February 1, 2019

Registration and abstract submission are available on our website: [www.texasmicroscopy.org](http://www.texasmicroscopy.org)

**Workshop - Thursday, Feb 21, 2019**

Workshops at UTSA Kleberg Advanced Microscopy Center

1. In situ TEM (sponsored by Franchini)
2. Confocal Laser Scanning Microscopy (sponsored by Rick)
3. Sample Preparation for SEM/EDS

[www.texasmicroscopy.org](http://www.texasmicroscopy.org)

## The 54<sup>th</sup> Texas Society for Microscopy Meeting February 21-23, 2019, San Antonio, TX





**\*\* Next TSM Meeting \*\***

February 20 - 22, 2020

[Click Here](#)

Hilton Conference Center  
College Station

hosted by  
Microscopy and Imaging  
Center  
Texas A&M University



[TSM is on  
Facebook!](#)



**TSM Meeting College Station - Feb 20-22, 2020**

[Click here for Registration](#)

[Click here to download the Final Program and List of Posters](#)

[Click here for further information and final call](#)

**Texas Society for Microscopy (TSM)**

The Texas Society for Microscopy (TSM) was founded in 1963 and has become an informative resource for many scientists since then. We welcome microscopists, researchers, students and administrators from all disciplines and backgrounds who are interested in microscopy or the science of microscopy.

Our non-profit organization is committed to advancing knowledge and understanding of all aspects of microscopy and their applications as they apply to life sciences, materials sciences and industry. We are committed to support students through our [Small Grant Program](#) and through travel grants to attend our annual meetings. The society is also represented at the meetings of the Microscopy Society of America through our president. The [annual meetings](#) of the TSM are a highlight for our members and enjoy wide corporate support.

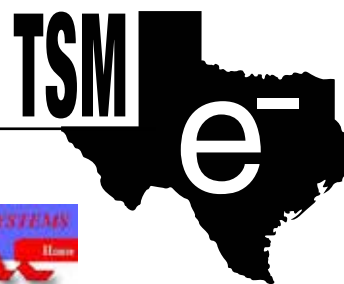
We invite you to become a member of the TSM and support its mission and vision through your [membership](#).



© 2020 Texas Society for Microscopy

Check out our new web page, [www.texas.microscopy.org](http://www.texas.microscopy.org), starting in March 2020!

# Corporate Members and Regional Sales Managers



**Advanced Microscopy Techniques**  
<http://www.amtimaging.com>  
242 West Cummings Park  
Woburn, MA 01801  
508-221-4449



**CARL ZEISS SMT**  
<http://www.zeiss.com/nts>  
One corporation Way  
Peabody, MA 01960  
978-826-1500  
978-532-5696 Fax



**IXRF Systems**  
<http://www.ixrfsystems.com>  
10421 Old Manchaca Rd., Suite 620  
Austin, TX 78748  
512-386-6100  
512-386-6105 Fax



**AMETEK (EDAX, Inc.)**  
<http://www.ametek.com>  
392 East 12300 South  
Suite H  
Draper, UT 84020  
201-466-0907



**Electron Microscopy Science/Diatome**  
<http://www.emsdiasum.com/microscopy/>  
1560 Industry Road, P.O. BOX 550  
Hatfield, PA 19440  
800-523-5874  
215-412-8450 Fax



**Solutions for Innovation**  
**JEOL USA, Inc.**  
<http://www.jeolusa.com>  
13810 Paisano Circle  
Austin, TX 78737  
978-495-2176



**AVR Optics**  
[www.avr-optics.com](http://www.avr-optics.com)  
187 N Water Street  
Rochester, NY 14604  
585-445-7588



**E.A. Fischione Instruments, Inc.**  
<http://www.fischione.com>  
9003 Corporate Circle  
Export, PA 15632  
724-325-5444



**Leica Microsystems, Inc.**  
<http://www.leica-microsystems.com>  
7125 Northland Terrace N., Suite 100  
Brooklyn Park, MN 55428  
314-374-9361



**BioTek Instruments, Inc.**  
<http://www.biotek.com>  
100 Tigan Street  
Winooski, VT 05404  
847-757-3387



**Gatan, Inc.**  
<http://www.gatan.com>  
5794 W. Las Postias Blvd.  
Pleasanton, CA 94588  
512-657-0898  
925-463-0504 FAX



**M.E. Taylor Engineering, Inc.**  
<http://www.semsupplies.com>  
SEM Micro Division  
15817 Crabbs Branch Way  
Rockville, MD 20855  
301-975-9798



**Bruker AXS, Inc.**  
[www.bruker.com](http://www.bruker.com)  
3194 Beverly Court  
Murrysville, PA 15668  
908-419-8225  
Austin, TX 78747



**Hitachi High Technologies America**  
<http://www.hitachi-hta.com>  
1375 North 28th Ave.  
PO Box 612208  
Irving TX 75261  
214-537-2158  
972-615-9300 Fax



**Micro Star Technologies, Inc.**  
<http://www.microstartech.com>  
511 FM 3179  
Huntsville, TX 77340  
936-291-6891 or 800-533-2509



Molecular Devices  
<https://www.moleculardevices.com/>  
 3860 North 1st Street  
 San Jose, CA 95134  
 469-662-8381



Rigaku  
[www.rigaku.com](http://www.rigaku.com)  
 9009 New Trails Dr.  
 The Woodlands, TX 77381  
 281-362-2300 ext. 122



Thermo Fisher Scientific  
<https://www.thermofisher.com>  
<http://www.fe1.com>



Nikon Instruments Inc.  
<http://www.nikoninstruments.com>  
 1300 Walt Whitman Road  
 Melville, NY 11747-3064  
 972-693-7779



RMC Boeckeler  
<http://www.rmboeckeler.com>  
 4650 Butterfield Drive  
 Tucson, AZ 85714  
 520-745-0001  
 520-745-0004 Fax



Tousimis  
<http://www.tousimis.com>  
 2211 Lewis Avenue  
 Rockville, MD 20851  
 301-881-2450  
 301-881-5374 Fax



Olympus Corp.  
[www.olympus-lifescience.com](http://www.olympus-lifescience.com)  
 48 Woerd Ave.  
 Waltham, MA 02453  
 512-230-5624



*Microscopy Products for Science and Industry*  
 Ted Pella, Inc.  
<http://www.tedpella.com>  
 PO Box 462477  
 Redding, CA 96049-2477  
 530-243-2200 or 800-237-3526



Oxford Instruments America, Inc.  
[www.oxford-instruments.com](http://www.oxford-instruments.com)  
 300 Baker Avenue, Suite 150  
 Concord, MA 01742  
 978-369-9933 x 201



PERFORMANCE IN HANDSPEECH  
 TESCAN USA, Inc  
<http://www.tescan-usa.com>  
 765 Commonwealth Drive, Suite 101  
 Warrendale, PA 15086  
 512-417-8990



Protochips  
[www.protochips.com](http://www.protochips.com)  
 3800 Gateway Centre Blvd., Suite 306  
 Morrisville, NC 27560  
 919-377-0898



Texas State University  
 Shared Research Operations  
<https://sro.txstate.edu/>  
 601 University Drive  
 San Marcos, TX 78666  
 512-245-6635



## What is PAMCELL™?

PAMCELL™ is a 3-dimensional cell culture plate which enables the formation of a wide range of uniformly sized spheroids. Plates are composed of hexagonally-arrayed spherical particles coated with cells adhesively controlled functional groups on the surface. These plates allow for the control of cell-to-substrate and cell-to-cell interactions.

- Enables formation of a wide range of uniformly sized spheroids
- Provides various patterns on a single plate without physical barriers
- Optically transparent for *in situ* microscopic observation in automated high throughput screening systems
- Easy to exchange culture medium (spheroids are stably attached on plate surface)

## PAMCELL™ Cell Culture Plates are available in two types

- **R Series Plates (96-well/6-well):**
  - R-100
  - R-600
- **T Series Plates (96-well):**
  - Test Culture Plate 1
  - Custom-made Plates

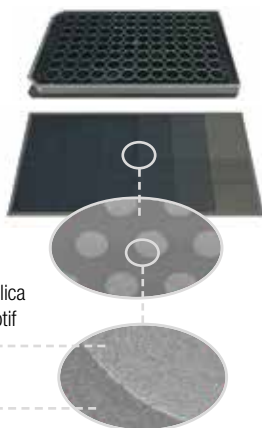
## Structure of PAMCELL™

**Lid:** Polystyrene, Clear  
**Body:** Polystyrene, Clear (USP Class VI tested)

**Substrate:** PET Film, Clear (100µm thick) or COP Film, Clear (188µm thick — fluorescence free)

**Particle:** Typically 700nm silica particle coated with ECM motif (ex. RGD) peptides

**Non-fouling Polymer:** (ex. PEG)



## R Series, 96-Well/6-Well Plates

For uniform, large spheroid production on a culture plate with uniform pattern and surface condition. Suitable for HTS Screening (Imaging automation).

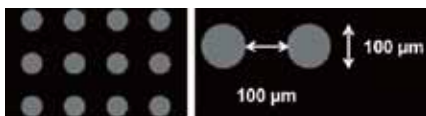
### Specifications

	R-100	R-600
<b>Micropad arrangement</b>	Square	Hexagonal
<b>Diameter of micropad (µm)</b>	100	600
<b>Gap between micropads (µm)</b>	100	200
<b>3D Spheroid formation</b>	Cell proliferation	Aggregation
<b>Spheroid production (spheroids/well or unit area)</b>		
96-well	800	60
cm <sup>2</sup>	2,500	180

1) Width of line: 3 µm w/48 lines

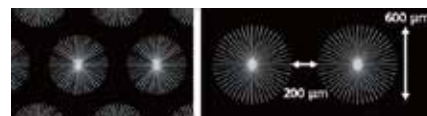


### R-100 Plate (Spheroid dia: 80~130µm)



- For small sized cells (ex. tumor cells)
- Anti-cancer drug screening (Ic50), Toxicity test
- Patient tumor cells + stromal cells co-culture

### R-600 Plate (Spheroid dia: 150~300µm)



- For primary cells (ex. fibroblast, stem cells)
- Regeneration medicine (cell printing, cell therapy)

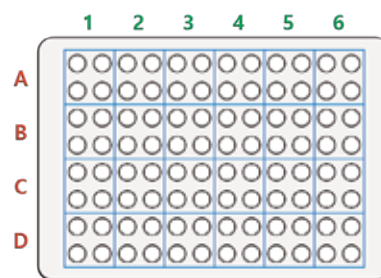
## T Series, 96-Well Plates

### Test Culture Plate 1

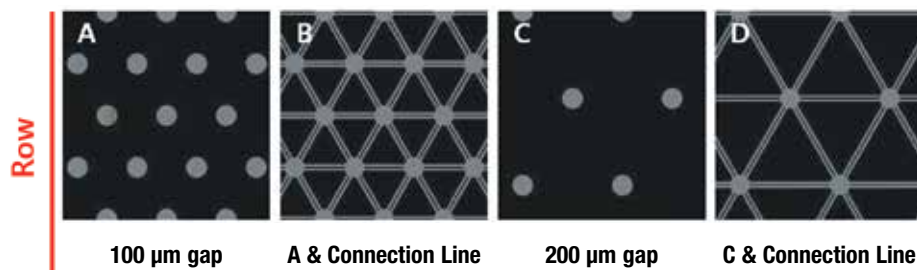
For wide ranges of spheroid size and spheroid networking.

### Custom-Made Plates

User's requested design plate (select from the Test Culture Plate 1 or new user-designed pattern).



Column	1	2	3	4	5	6
<b>Circle Dia. (µm)</b>	50	100	150	200	250	400



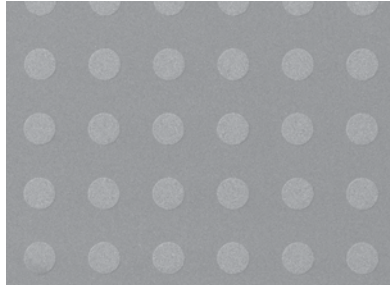
## Ordering Information

Cat. No.	Description	Qty.
64830-01	R Series 96-well Plate	each
64830-02	R Series 6-well Plate	each
64830-03	Test Culture Plate 1	each
64830-05	Custom-made Plate	each

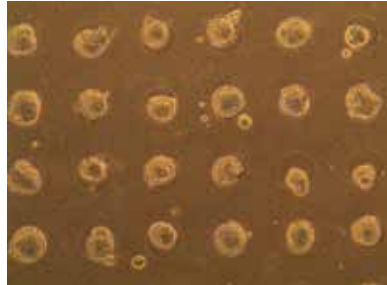
# Applications

## Spheroids (tumors, stem cells)

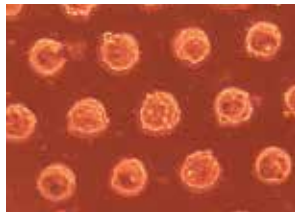
- HTS (Anti-cancer, Toxicity), Disease models
- Tissue spheroid mass production (~800 spheroid/96-well)



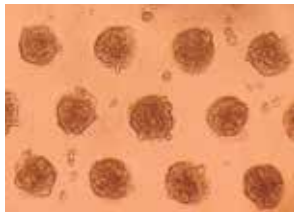
R100



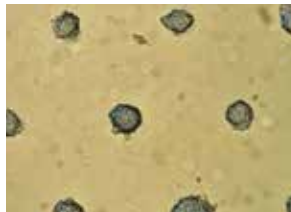
HT-29 (Colon)



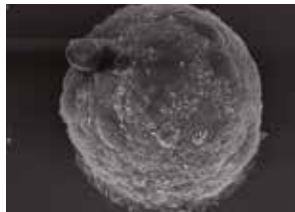
FaDu (Pharyn)



A549 (Lung)



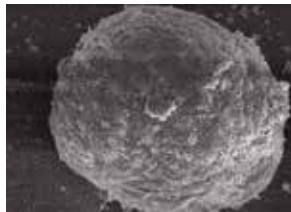
SH-SY5Y (Nerve)



FaDu (Pharyn)

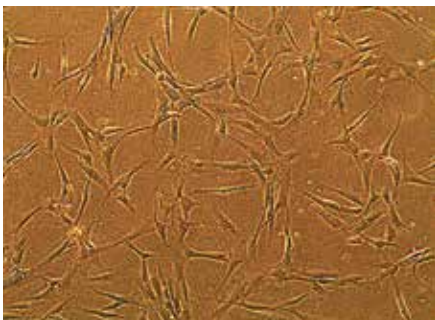


A549 (Lung)



HT-29 (Colon)

## ADSC — Serum-free



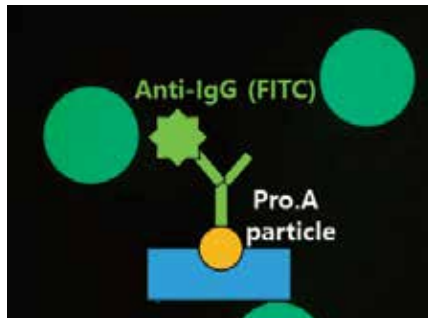
## Whitening Test



## Chondrocyte Pellet



## Surface Marker



## Single Cell Assay (Response/Differentiation)

### Adipose Derived Stem Cells (ADSC)



## Electron Microscopy Sciences

P.O. Box 550 • 1560 Industry Rd.  
Hatfield, Pa 19440  
Tel: (215) 412-8400  
Fax: (215) 412-8450  
email: [info@emsdiasum.com](mailto:info@emsdiasum.com)  
or [stacie@ems-secure.com](mailto:stacie@ems-secure.com)

OUR MAIN INTERACTIVE WEBSITE:  
[www.emsdiasum.com](http://www.emsdiasum.com)

 TO REQUEST A COPY  
OF OUR CATALOG:  
[www.emsdiasum.com/  
requests/catalog](http://www.emsdiasum.com/requests/catalog)

 TO VIEW OUR  
DIGITAL CATALOG:  
[catalog.emsdiasum.com](http://catalog.emsdiasum.com)

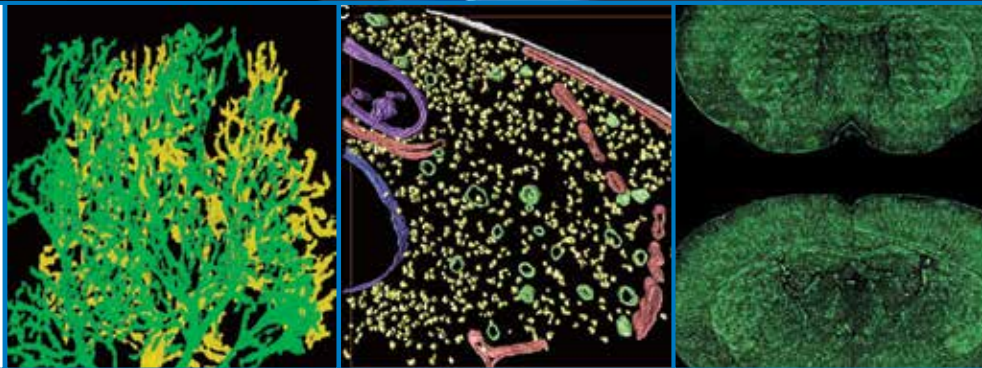
 ...OR SCAN HERE:



# DiATOME Diamond Knives



at the forefront of innovation



**NEW! Ultra ATS** The Ultra ATS Diamond knife is perfect for placing sections on Si wafers to view under the SEM. The knife comes in 3.0mm size with 35° angle.

**ultra 45° • cryo • histo • ultra 35°  
histo jumbo • STATIC LINE II • cryo immuno  
ultra sonic • ultra AFM & cryo AFM  
trimtool 20, 45, and 90**

[www.emsdiasum.com](http://www.emsdiasum.com)

**DiATOME U.S.**

P.O. Box 550 • 1560 Industry Rd. • Hatfield, PA 19440  
Tel: (215) 412-8390 • Fax: (215) 412-8450  
email: [info@emsdiasum.com](mailto:info@emsdiasum.com) or [stacie@ems-secure.com](mailto:stacie@ems-secure.com)